An investigation of automotive springs: ageing effects

A thesis submitted to The University of Manchester for the degree of Master of Philosophy in the Faculty of Sciences & Engineering

2016

Alejandro Perez Hernandez

School of Materials

Contents

Total word count 21,290

List of Figures

List of Tables

List of Equations

The University of Manchester
Alejandro Perez Hernandez
Master of Philosophy
An investigation of automotive springs: ageing effects
July 2016

Abstract

This work aims to simulate and compare the spring performance before and after corrosion. The microstructure of a material commonly used by the spring automotive industry, 54SiCr6 alloy steel is analysed.
A finite element model was created to simulate a spring performance under design conditions, a 16 millimetres (mm) coil diameter and a static load of 2255 N; which represents the proportional weight of an automobile in a stationary condition. Based on the analysis of corroded samples and observing how the corrosion progress affecting the material, a second model was created with a coil diameter reduction of 1 mm, with the objective to compare the performance between the models.
It was observed the reduction on the coil diameter increased the stress of the material by 25% at the highest value, and the deflection has an increased by almost 20 mm under the same load; diminishing the spring performance as expected.

Declaration

No portion of the work referred to in the thesis has been submitted in support of an application for another degree or qualification of this or any other university or other institute of learning

Acknowledgements

The author would like to express his grattitude to Consejo Nacional de Ciencia y Tecnologia (CONACyT) for the funding of this work. Jaguar Land Rover and the Jaguar Land Rover technical staff, for many helpful discussions, and advice. Dr. Clara Frias, Prof. Xiaorong Zhou, Dr. Mazher Yan and Dr. Ying Wang for guidance and support.

Nomenclature

α	End coil condition
β	Shape parameter
δ	Spring deflection
η	Scale parameter
ν	Poisson's coefficient
π	Pi
σ	Torsional stress
τ_{all}	Allowable stress
A	Intercept
a_0	Threshold of the pit size
C	Spring index
D	Spring mean diameter
d	Wire diameter
E	Energy

F	Force
G	Shear modulus
H	Height
k	Spring rate
K_B	Bergsträsser factor
K_C	Curvature correction factor
K_S	Shear stress factor
K_W	Wahl factor
L	Load
L_O	Free length
L_S	Solid length
m	Slope
N_a	Number of active coils
N_t	Total number of coils
r	Spring mean radius
S_{sy}	Distortion energy torsional yield strength
S_{UT}	Minimum tensile strength
S_{ys}	Torsional yield strength
v	Velocity
m	Mass

Chapter 1

Introduction

1.1 General background

Springs appear in history on the first age of technology, equipment that worked for food gathering were developed. First springs were made out of vegetable fibres, when the bronze age surged new materials became available therefore new applications were possible. In the renascence several structures used springs, such as catapults improved by Leonardo Da Vinci who started a catalogue of springs. In the late 16th century the springs were used in more complex machines, and in the 18th century the french included a metal plate under a carriage. This is considered now as a leaf spring and the first one to be used on a vehicle [1]. This research focus solely on automobile suspension springs and the simulation of the spring behaviour and performance.

1.2 Current state

In the early years of the automobile industry when a component was inadequate a common practice was to increase the thickness to create a more robust and heavier design to accomplish the rougher conditions. Today this is not a possibility since the efficiency of the automobile is considered to be one of the most important aspects. Each piece of the vehicle must not only meet the requirements for which it was designed but also do it in the most efficient way. An alteration in the basic component such as the material or the design will help on how to solve the problem. Automobile manufactures are opting to change the raw materials, due to social consciousness, environmental sustainability or legal requirements imposed by governments.

Automobiles are complex products and consist of thousands of pieces. Some parts behave independently, while others are completely dependent of different parts to operate. Automobiles deal with many operational and environmental variables. Such problems are difficult to evaluate, since the service conditions where the vehicle operates, can not be exactly specified or clearly quantified. The variation of these conditions are contemplated in a range that is representative of what the automobile is expected to deal with.

1.3 Automobile operation environment

Due to the grand variety of commercial routes, it is possible to export manufactured products to most parts of the world. This is the reason why there is a greater demand for attention on the environment in which the automobile will perform. Now it is expected for an automobile to be exposed to extreme operation conditions, from the cold winter weather near the polar circle, to the arid and hot deserts of the world, and the humid and corrosive cost line environments. To help understand the attack of the environment on the springs, Figure 1.1 presents a measurement of marine salt displacement, which under appropriated conditions can travel more than 50 kilometres inshore [2].

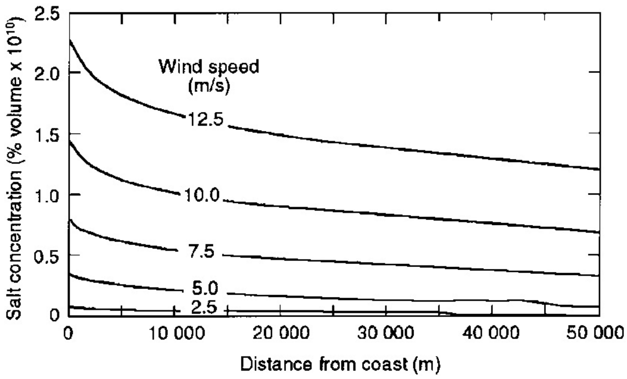

Figure 1.1: Percentage of salt concentration on coast line [2]

Not only the natural environment present a challenge for the automobiles, urban areas present also special situations. An example could be on the northern region of the globe, where most countries have annual blizzards and snowfall. The solution for the snow accumulation on the streets, is a maintenance procedure based on salts deposition on roads, Figure 1.2. Trenouth et al. [3] exposed in their work the salt accumulation on roads, which in turn increases the ageing of the automobiles materials, as they are exposed to this created environment condition.

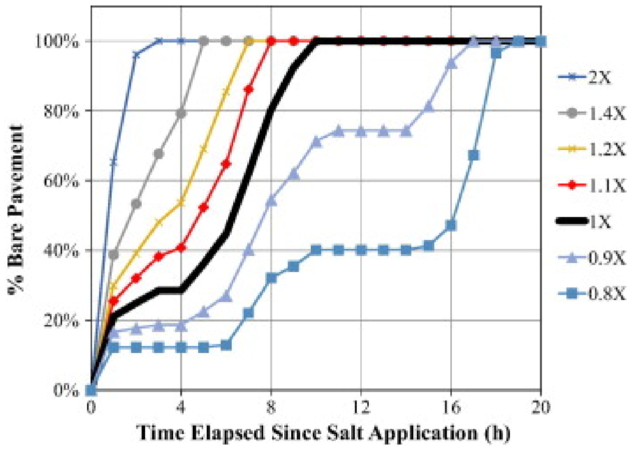

Figure 1.2: Ice melting time from salt concentration on road [3]

The wide range of temperature operations, humidity percentage and saline concentrations among other environmental factors will produce a rapid wear down of the automobile parts. It is of vital importance to understand the behaviour of the materials in such conditions.

1.4 Areas of improvement

For years the automobile designers have faced the challenge to optimise the performance and efficiency of the automobiles. A way to improve performance without increasing the fuel consumption is weight reduction on the automobile parts, however the weight reduction should not compromise the mechanical properties.

The necessity of lightweight materials or upgrade the existing designs are fundamental keys on the manufacturing of new automobile parts. It has been mentioned that as for every 10% of weight eliminated from a vehicle's total weight, fuel economy improves by 7% [4].

New regulations [5] have also taken place on the importance in fuel consumption and greenhouse gases reduction. These type of regulations have lead car manufactures to improve the efficiency of their automobiles and create hybrid or electric automobiles. It has been estimated that for every kilo-gram of weight reduced in a vehicle, there is about 20 kg of carbon dioxide reduction [4]. There is also the need to fulfil with the new laws for end of life vehicles [6]. These laws, dictate the amount of material that can be disposed at the end of the life cycle of the automobile. It is stipulated in the new regulations that a producer must achieve a 95% of reuse and recovery target, and a 85% reuse and recycling target of the weight of the vehicle for which the manufacturer has declared responsibility [6]. These new factors are used as input for new designs and material selections for the automobile industry.

1.5 Objectives and scope of research

The aim of this research is to simulate the performance of an automobile suspension spring. Simulations before corrosion and after corrosion were compared. The differences of the models were based on the analysis of corroded samples.

Particular or specific objectives:

- Analyse the microstructure composition of the spring material in search of defects or impurities.
- Understand the mechanism of corrosion on the spring and what could trigger it or provoke it.
- Create a reliable simulation model on spring performance with design properties.
- Determine the change of spring performance and material stress increase due to corrosion, when under static mechanical loading.
- Compare simulations to quantify the change in performance of the spring.

1.6 Concluding remarks

In this chapter a glimpse of the path the springs have made in order to obtain the role they have today in society is reviewed. New variables, such as regulations, that impulse the necessity of improvement are some of the reason springs continue to evolve.

It is mentioned the service conditions where springs perform plays an important role, as it interacts continuously with the spring during its life cycle. These effects are non-controllable, reduce the life expectancy, and increase the probability of a premature failure.

New proposals and developments have to be taken into consideration for the increase of efficiency and performance required by regulators. The use of a lightweight material presents a promising solution for weight, efficiency, performance, and the new requirements that had been established.

Chapter 2

Literature review

2.1 Introduction

In order to create a reliable simulation of the spring, different topics needed to be taken into consideration. The basic principles of spring performance are presented. The mechanical properties that can affect spring performance are identified. Spring design is based on geometry, material, and load applied, and these variables need to be considered in order to obtain a satisfactory performance.

Another important topic to understand is the material natural response to corrosion. The different types of corrosion will be reviewed. The understanding of the triggering conditions that lead to corrosion will be studied, and also what can be done to minimise these conditions.

Previous finite element modelling simulations were reviewed and analysed. Valuable information regarding the reliability of the simulation was obtained from these works.

2.2 Suspension springs

2.2.1 Function of springs

Springs are flexible devices used to exert force or torque, and store energy. The force produced by a spring can be compressive or tensile, and linear or radial. The process of deflecting a spring involves the transfer of energy into stored spring energy. When the force causing the spring deflection is removed, the stored spring energy will return the spring to its original position. Springs can be classified by the direction and nature of the force exerted when they are deflected [7]. In general the main functions of the springs are the following:

- To absorb energy and reduce shock. The spring must retain most of the energy flowing to the system therefore the spring must deflect a considerable amount to avoid any peaks.
- To apply a definite force or torque. This could be used to maintain a specific degree of force regardless of the change in the environment operational conditions, such as temperature pressure or vibration.
- To support moving masses or isolate vibration. This is mainly to reduce energy going to a system generated from an impact or vibration.
- To indicate or control load or torque. One of the most recognised uses is as a flexible member that deflects when subject to a force or torque.
- To provide an elastic pivot or guide. In some situations a system of springs may have an advantage over bushing because of the low internal friction [8].

Most of the applications are comprehended on the categories presented in Table 2.1. However they are still customised applications that may not fit into any of these categories. Such applications are usually for springs with non-linear load deflection behaviour.

Table 2.1: Classification of springs based on the force or torque exerted [7].

Actuation	**Type of spring**
Compressive	Helical compressive springs Bellevile springs Flat springs
Tensile	Helical extension springs Flat srings Draw bar springs Constant force springs
Radial	Garter springs Elastomeric bands Spring clamps
Torque	Torsion springs Power springs

2.2.2 Types of mechanical suspension springs

In general, springs may be classified as wire springs, flat springs, or special-shaped springs, and there are variations within these divisions [9]. Wire springs include helical springs of round or square wire, made to resist and deflect under tensile, compressive, or torsional loads. Flat springs include cantilever and elliptical types, wound motor or clock-type power springs, and flat spring washers, commonly called Belleville springs. [9]

Leaf springs, originally called laminated or carriage spring, are a simple form of spring, regularly used for the suspension in wheeled vehicles. It is one of the oldest forms of springs, dating back to medieval times, sometimes referred to as a semi-elliptical spring or cart spring. These springs take the form of a slender arc, usually of rectangular cross-section [10]. The centre of the arc provides location for the axle, while tie holes in the edges called eyes, are provided for connection to the vehicle body. For very heavy vehicles a leaf spring can be made from several leaves stacked on top of each other in several layers, often with progressively shorter leaves [10].

Another category is the helical spring, which in turn may be subclassified depending on its profile shape. The most characteristic representation of the helical springs is the continuous rod or wire wrapped into a cylindrical form with a specific pitch between adjacent coils. This kind of profile shape can have different diameters or profile figures depending on the design that is required on the usage conditions [7].

In Figure 2.1 the geometric characteristics that need to be specified to clearly categorise a spring are shown. This also help to establish the range on which it may be operational. It is not necessary that every single spring fits into a category. There are specific applications that required a spring design with a unique shape and behaviour, to fulfil a rather specialised task.

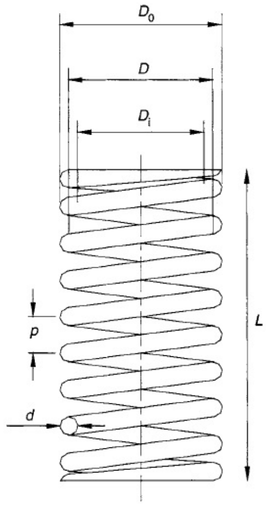

Figure 2.1: Representative dimension of helical springs [7]

The representative dimensions in a spring are L_0 as the free length or total length of the spring, d is the wire diameter, which can be constant or variable, p is the pitch or distance between coils, D is the mean coil diameter, D_O is the outside diameter of the spring, and D_I is the inside diameter of the spring.

Most of the helical springs will fit into one of the profile shapes listed in Figure 2.2 as these are the most common shapes. The requirements of space, loading range, load condition, and material properties make this geometries suitable for most of the duties. It may exist some exceptions where the profile geometry can be arranged in a different shape for a very specific purpose.

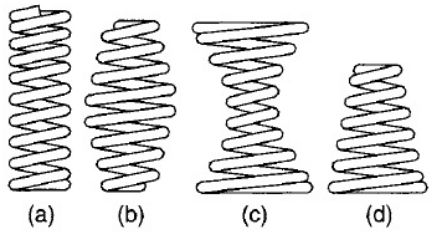

Figure 2.2: Types of spring shapes (a)variable pitch (b)barrel (c)hourglass (d)conical [7].

On helical springs the cross section shape of the wire is frequently a circular shape, however it can also be employed a square section or a rectangular shape well. The variation of the cross section depends on the space available for the spring, the material presentation, manufacturing process, or design requirements [8]. In Figure 2.3 it can be seen the difference between the cross section types of springs.

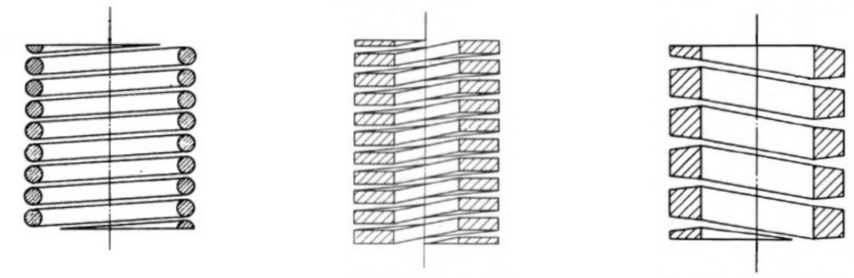

(a) Circular (b) Rectangular (c) Square

Figure 2.3: Cross section of helical springs with different wire.[8].

Another characteristic of the springs is the end type of the wire used for the helical springs. The influence of the end type is significant on the immediate response of the spring behaviour against the load condition. The most common end coils are plain, squared and ground end, Figure 2.4 [9].

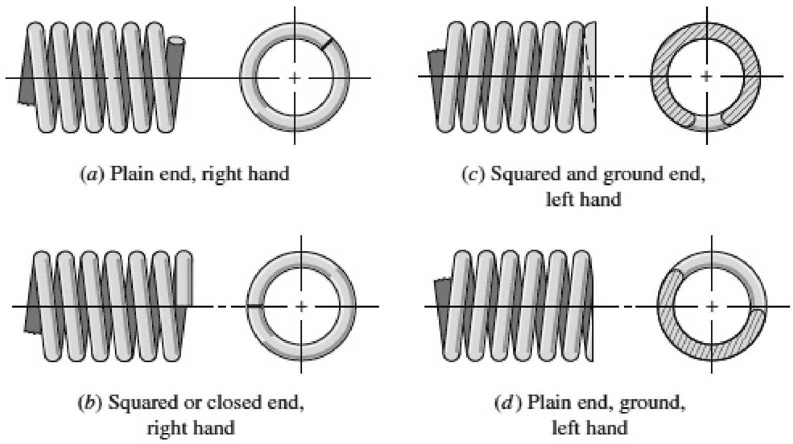

Figure 2.4: Geometry of four standard helical compression springs types [9].

Some of the main differences between the end types of the springs are based on the response they produce at the moment the load is applied on the spring, an example of different ends are:

- Springs with plain ends have no interrupted helicoids at the ends, and are the same as if a long spring had been cut into sections.

- A spring with squared and ground ends compressed between rigid plates can be considered to have fixed ends.
- A spring with plain ends that are squared or closed is obtained by deforming the ends to a zero-degree helix angle.
- Springs should consistently be both squared and ground for important applications, because a better transfer of the load is obtained.

The geometry of the spring used in automotive suspension (Figure 2.5) varies depending on the design. A common geometry of spring is a conical, variable pitch, round wire, with closed ends.

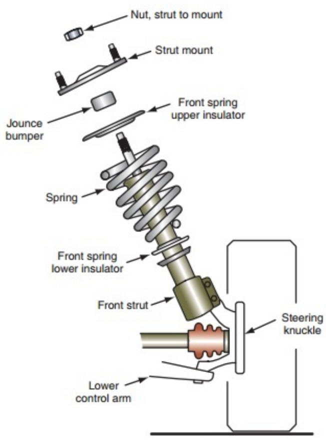

Figure 2.5: Typical MacPherson strut front suspension system [11].

It is important to mention that tailor design can accomplish an unique purpose. A new design of a spring configuration was made to have a composed spring with two different profiles [12]. A spring was created (Figure 2.6) by Watanabe et al. [12] where a single spring mixed both characteristics and behaviour of two different kinds of geometry. A second auxiliary spring regularly is used to help reach contact with the main spring and the seat. In this spring it was proved that stress distribution did not focus at the torsion area where the springs join, but it spread through the all component in a linear response. In this configuration it was still possible to obtain a non linear displacement as such, which was the desired behaviour of the spring [12].

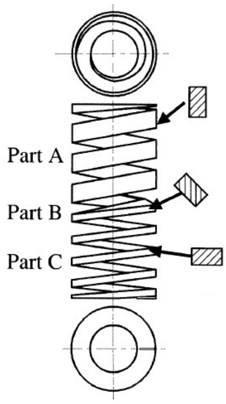

Figure 2.6: Composed spring with auxiliary spring [12].

2.2.3 Selection of spring materials

Virtually any material can be used to make springs, however the ideal material needs to have a high ultimate strength, a high yield point and a low modulus of elasticity, in order to provide maximum energy storage [7]. Possible alternative materials include high strength steels, glass fibre reinforced polymer (GFRP), titanium alloys, glass and nylon, among others. The choice for most applications tends to be limited to plain carbon steels, alloy steels, stainless steels, high-nickel steels, and copper-based alloys.

Most spring materials are manufactured according to American society for testing and material (ASTM), British standard (BS) or Deutsches institut für normung (DIN) specifications. Provided the material is not stressed beyond the elastic limit, the usual type of spring will have a straight line load vs deflection diagram [7].

Important aspects in spring design include determination of the spring material and dimensions. This is in order to ensure the spring will not fail due to either static or variable loads. One requirement for springs design is that it will not buckle or deform under the load within allowable limits.
The material natural frequencies of vibration, are generally, sufficiently higher than the frequency of motion the springs will control [7].

Since all materials deform with load, in a spring the parameter of this feature is called spring rate. It is defined as the slope of the force deflection curve of a spring. If the slope is constant then the Equation 2.1 can be employed, where k is the spring rate, F is applied load and δ is the deflection.

$$k = \frac{F}{\delta} \tag{2.1}$$

According to Shigley [9], one way to calculate the deflection of the spring is with the formula

$$\delta = \frac{64 F r^3 N_a}{d^4 G} \tag{2.2}$$

which is based on the properties of the material and the geometry, where G is the shear or torsional modulus and N_a is the active number of coils, r the mean diameter from the spring, d the coil diameter (Figure 2.1), and F the load applied on the spring.

The spring rate is also known as the spring constant or spring scale. Spring rates can be linear or nonlinear and it is the representative value of how the spring will behave under loading conditions.

The springs are subject to a relative large amount of energy they need to store, deflect, or transmit. The best results are obtained at high working stress. This demonstrates why most spring materials have high tensile strength and work at higher stresses than in other fields [8].

The most widely used material for springs is carbon steel. The smallest size of wire with a 0.8-0.9% carbon steel by cold drawing and forming is known as music wire, usually between 0.01-0.16 in. diameter [8]. Usually using 1 per cent carbon steel the material is cold treated after forming to obtain a higher ultimate strength. Similar values of ultimate strength can be obtained as those for the 1 per cent carbon steel from chrome-vanadium alloy steel [8]. In larger diameter sizes, helical springs are commonly treated after forming, the latter frequently been done hot. After winding a stress relieving low-temperature heat treatment is usually given [8].

Another common material is the stainless steel spring of 18% chromium, 8% nickel composition, occasionally chosen when corrosion effects are present or for high temperature applications. Phosphor bronze is also used where corrosion is present, however this material has a considerably less strength than stainless steel [8].

One of the major problems springs need to tackle, is the presence of corrosion. One approach [13] is the substitution of steel in production of springs for a corrosion resistant material. The change of material will produce a change in the value of shear modulus (G), this change must be compensated by alterations in coil diameter, mean diameter, or number of active coils [14].

2.2.4 Types of loading

It is commonly expected have different load situations on springs, such as static, variable, and sometimes a third situation may be present, known as impact (Table 2.2). First situation is a static load, which can be tension load or compression load. Tension loading means the spring is required to avoid the separation of the adjacent parts. Compression loading is when the loading or deflection of the springs is constant for most of the life of the spring. Only a few times in their lifetime they will be freed from such load, these springs are known as statically-loaded springs.

Table 2.2: Load types on springs [9].

Types of loading	**Description**
Static	Constant and invariable load
Variable	Load usually applied within a previous known range of values
Impact	Load applied abruptly and at high speed for an instant

A consequence of tension springs charged for a large amount of time is called settage, this affects springs with plastic deformation of the material. Another consequence that occurs in springs subjected to a large amount of time on deflection state is known as relaxation. The loss of response to load may be present, while a small loss can be tolerated, too much will cause the spring to be ineffective. At normal temperatures if the peak stress of the spring material is maintained under the elastic limit, any of these phenomenons rarely occurs.

The second situation is the variable loading. This is when the load magnitude does not remain constant, and can be either tension or compression loading. Usually the spring will work between a range of a minimum and maximum stress, or load. The third possible situation a spring may encounter, depends on the task. The impact loading, generally presents on the variable load springs, occurs in a more dynamic environment. In this case the load or tension is applied in just a moment but with a force significantly larger than the regular range of operation for the springs.

2.2.5 Fundamentals of spring design

The Hooke's Law is a keystone in springs design; it states the deflection is directly proportional to load as long as it is within the elastic limit [15].

There are steps that can be followed to design springs and calculate their dimensions based on the expected load. For the most common raw material used in spring design, mechanical properties had been reported. Tables had been made to reduce the calculation time for a spring. The use of tables may not be as precise as using the equations but still provide an acceptable result. The values obtained from tables can then be iterated to a more precise result in the design of the springs.

In order to realise an accurate design of springs, the material that will be used must be taken into consideration, the environment conditions for that spring, and the work load. The design of the springs are directly linked to the mechanical properties of the materials. The environment in which the springs will work affect directly and significantly the mechanical properties. Considerations need to be included as part of safety factors in order to create a good design. A visual representation of the steps can be seen in Figure 2.7.

In the process of spring design it must be taken into consideration important factors, the most known property of a material is the maximum tensile stress (S_{UT}). This value can be taken from a tensile test to which most materials are subjected to. Most of these result values are usually catalogued. Some of the most important values that are needed are, the Young modulus (E) and the shear modulus (G). These values will help to calculate the Poisson ratio (ν) with Equation 2.3, [16]. An analysis can be performed to determine the behaviour of the material which will help to obtain a satisfying design including the material properties. The outside factors that have a significant role in the design are the safety factors. They are used to maintain the specific mechanical characteristics of the material within the the possible range of values the springs should be able to comply.

$$G = \frac{E}{2\left(1+\nu\right)} \tag{2.3}$$

The material and the manufacture process also have an effect on tensile strength. The graph of tensile strength versus coil diameter is almost a straight line for some materials, specially iron or metallic alloys. When plotted on log-log paper, writing the Equation 2.4 of this line, represents a good mean of estimating minimum tensile strengths (S_{UT}), when the intercept (A) and the slope (m) of the line are known for a given coil diameter (d) [9].

$$S_{UT} = \frac{A}{d^m} \tag{2.4}$$

For those materials on which the values are not known for the slope and the intercept, for instance a carbon fibre reinforced polymer (CFRP) another procedure must be performed to determine the minimum tensile strength for an specific diameter. This value will help us to approve the required spring geometry based on the material information. The easiest way of obtain the values of maximum tensile strength would be to perform a tensile test on a

Define design problem

$\downarrow$

Select spring configuration

$\downarrow$

Select material

$\uparrow\downarrow$

Select stress level

$\downarrow$

Design to optimize

$\uparrow\downarrow$

Check design

$\downarrow$

Specify

Figure 2.7: Spring design sequence [17].

rod of the expected diameter of the material to obtain the data based on a reliability of the manufacturing process for this kind of material.

It is essential to obtain the working conditions in which the spring will be located, and determine if the load will be static or variable. In the event of variable loads the maximum value will be the choice for calculation, this is to assure the spring will be able to handle all the range of load without suffering plastic deformation or failure. The Equation 2.5 is used to determine the maximum value of shear stress (τ) in the material based on the force applied (F) the mean diameter of the spring (D) and the coil diameter (d).

$$\tau = \frac{8FD}{\pi d^3} \tag{2.5}$$

Maximum shear stress is composed of the combined stress applied on the wire material. A direct shear which is the result of the direct loading on the spring pushing all the spring down and the normal reaction that occurs create the shear stress. The second stress that is induced in the material is the torsion shear stress, this results from the actual twisting of the rod material. It creates an angular rotation of the material edge at the moment of the tension or compression due to the geometry which tends to be a dominant stress and specially on the inner side of the springs. It can be visualised on Figure 2.8 and the resulting representation of the combined stress is a more closer approach to the real conditions the material has to sustain. [8]

The Equation 2.5 does not take into consideration some of the additional stress caused by the curvature of the wire or the shear load, which depending on the mean diameter (D) tends to vary as well [15].

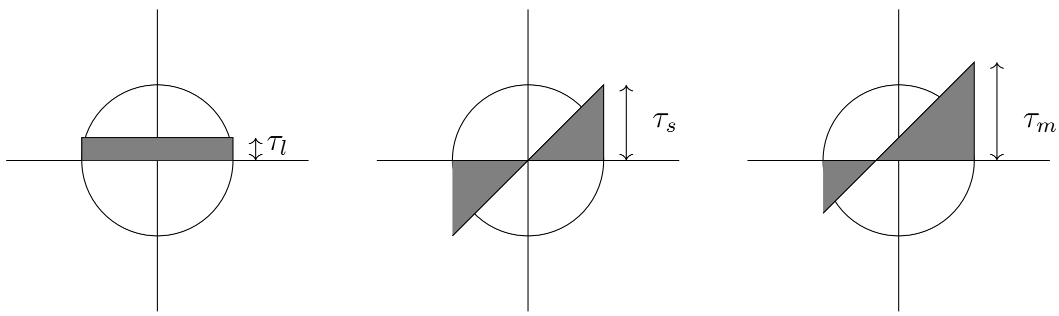

(a) Direct shear stress (b) Torsion shear stress (c) Maximum shear stress

Figure 2.8: Visual representation of direct shear (a), torsion shear (b) and combined shear (c) on the material [8].

In order to determinate the proper wire diameter (d) it must be used a torsional stress (σ) at a given load (L), commonly this can be calculated in approximation to give a value in the Equation 2.6. The size can be refined with a standard size or rod material or if the material allows it, the correct size of the wire can be determined [15].

$$d^3 = \frac{2.55LD}{\sigma} \tag{2.6}$$

In order to have more accurate value of the stress to which the material is subjected, it is necessary to include the curvature factor of the wire (K). Wahl [8] published a method of calculation where he determines and uses the Wahl factor (K_W).

$$K_W = \frac{4C-1}{4C-4} + \frac{0.615}{C} \tag{2.7}$$

Equation 2.7 was determined, where C is the relationship with the wire size and the mean diameter than can be obtained with Equation 2.8

$$C = \frac{D}{d} \tag{2.8}$$

Then the shear factor (K_S) is calculated based on the Equation 2.9.

$$K_S = \frac{2C+1}{2C} \tag{2.9}$$

With all this information it is possible to calculate the curvature correction factor (K_C) by the relationship 2.10

$$K_C = \frac{K_W}{K_S} \tag{2.10}$$

It was latter proved by Cyril Samónov [18] that another way to calculate the curvature factor was by using the Bergsträsser factor (K_B). The Equation 2.11 is used to obtain such value.

$$K_B = \frac{4C+2}{4C-3} \tag{2.11}$$

The difference between equation 2.7 and 2.11 is less than 1%, and this factor can be taken into consideration for a reduced calculation of the K_S [9]. On the equation 2.10 it is possible to decide to use either, K_W or K_B.

Finally the K_C is added to the Equation 2.5 and gives out the corrected version of stress (τ_{max}) on the material of the spring in Equation 2.12.

$$\tau_{max} = K_C \frac{8FD}{\pi d^3} \tag{2.12}$$

Next step in the design of the spring is to check if the spring will have enough room when in free length, usually under no load; or when the spring is under full load and reach solid length. The solid length of the spring, is the maximum displacement the spring can obtain. The solid length (L_S) can be calculated with the Equation 2.13 where N_t is the total number of coils on the spring.

$$L_S = (N_t + 1)d \tag{2.13}$$

Another way of calculating the number of coils in the spring is taking Equation 2.14 and calculate them based on a desired deflection (δ) [15]. It is possible to do so using the Equation 2.14, which uses the total number of active coils (N_a), δ and the nominal mean radius of the spring (r).

$$N_a = \frac{\delta G d^4}{64 F r^3} \tag{2.14}$$

It is important to remember in this case the number of coils given is the number of active coils. Based on the end of the coils as shown on Table 2.3, it needs to be calculated the correct amount for the total coil springs.

Table 2.3: Formulas for the dimensional characteristics of compression springs [17].

	Types of spring ends			
Term	**Plain**	**Plain and ground**	**Squared or closed**	**Squared and ground**
End Coils	0	1	2	2
Total coils	N_a	$N_a + 1$	$N_a + 2$	$N_a + 2$
Free length	$pN_a + d$	$p(N_a + 1)$	$pN_a + 3d$	$pN_a + 2d$
Solid length	$d(N_t + 1)$	dN_t	$d(N_t + 1)$	dN_t
Pitch	$(L_o - d)/N_a$	$L_o/(N_a + 1)$	$(L_o - 3d)/N_a$	$(L_o - 2d)/N_a$

Continuing with the calculation the maximum load that the spring can sustain without presenting buckling can be estimated. This is a very useful measure because if buckling is detected, it means the design geometry of the spring may not reach its full potential. It will probably fail prior to be completely compressed and then it would be needed to make a selection of a different material or geometry to avoid this kind of problem. To calculate the stability of the spring, the Equation 2.15 presented by Wahl[8] is used, where L_0 is the free length, α is the end condition of the spring and a value can be taken from the Table 2.4, D is the mean diameter, and the values for Young modulus (E) and shear modulus (G) correspond to the mechanical properties of the spring material.

$$L_O < \frac{\pi D}{\alpha} \left[\frac{2(E - G}{2G + E} \right]^{\frac{1}{2}} \tag{2.15}$$

Once these calculations have been done, considerations need to be taken, like the magnitude of the load the spring will be subjected to. For safety reasons the highest load should always be considered, even if it's not a common circumstance in the spring life cycle. Failure to sustain such loads could produce catastrophic results.

Table 2.4: End condition constants α for helical compression springs [9].

End condition	**Constant** α
Spring supported between flat parallel surfaces (fixed ends)	0.5
One end supported by flat surface perpendicular to spring axis (fixed),other end pivoted (hinged)	0.707
Both ends pivoted (hinged)	1
One end clamped; other end free	2

As described before, Equation 2.1 can be used to calculate the spring rate, another equation that can be used is 2.16. This can also give a value that will help on the determination of the spring design in the event the deflection is not available or it was not previously calculated. It is useful as it will provide information on the behaviour that the spring should have based on the properties on the material.

$$k = \frac{d^4 G}{8D^3 N} \tag{2.16}$$

Based on the configuration of the spring ends it may differ, however it is possible to determine this value according to Table 2.3.

So far the main components on the springs have been determined, having the spring wire diameter, number of coils and length of the spring as the most indicative characteristics of the geometry. It is still important to remember that the material plays an important role on the performance of the spring. It is vital to make sure the material will hold the stress of the load.

One important consideration is the springs must never be designed to be compressed completely in their working travel. This will result in wear from coil clash and can induce a premature failure [15].

Most of the materials are only tested on tensile test, but in order to calculate the torsional yield strength the Equation 2.5 can be used. It can be assumed that the tensile yield strength is between 60 and 90 percent of the tensile strength [9]. Depending on the method, one possibility is the calculation of the distortion energy theory, also known as Mises [19]. This theory uses Equation 2.17 to state the torsional yield strength (S_{ys}).

$$S_{ys} = 0.577 S_y \tag{2.17}$$

The torsional yield strength (S_{sy}) with the distortion energy theory can be then calculated with the Equation 2.18.

$$S_{sy} \geq 0.50 S_{UT} \tag{2.18}$$

There are still another set of possible paths for calculation, for example the Joerres Equation 2.19 with an approach where the author takes the maximum allowable torsional stress for static applications and the value of $S_{sy} \geq 0.65 S_{UT}$ and claims strength may increase through cold work [9]. Using Equation 2.19 it is possible to obtain such result.

$$S_{sy} \geq 0.65 S_{UT} \tag{2.19}$$

Another method to obtain a value presented by Samónov [20] where discussion of allowable stress (τ_{all}), shows for high tensile spring steels the Equation 2.20.

$$S_{sy} = \tau_{all} = 0.56 S_{UT} \tag{2.20}$$

The author also note that the values obtained for allowable stress is specified by Draft Standard 2089 of the German Federal Republic when Equation 2.5 is used without a shear factor. This will lead to the formula 2.21 for this approach.

$$S_{sy} \geq 0.56 S_{UT} \tag{2.21}$$

Once the values have been obtained for the minimum tensile strength and torsional yield strength of the material they can be used to compare with the values for the load conditions. This comparison will define if it is needed to re-design the spring or it can be expected the spring will have a good performance with the defined load.

One thing to keep in mind is that all of these Equations and calculations are based on the fact that the loads are applied slowly, therefore the speed of the load applied is not taken into consideration. The speed in which the spring will compress is generally not an easy information to obtain or even estimate, unless it is a continuous manufacturing process where it can be calculated [15].

Equations specially for loads suddenly applied exists, such as Equation 2.22 for sudden load, and for loads dropped from a given height is Equation 2.23 [15].

$$\delta = \frac{2F}{k} \tag{2.22}$$

$$\delta^2 = \frac{2F(H+\delta)}{k} \tag{2.23}$$

Where the Equation 2.23 will produce a result as a quadratic equation of the form $ax^2 + bx + c = 0$ and can be solved with the quadratic formula [21].

$$x = \frac{-b \pm \sqrt{b^2 - 4ac}}{2a} \tag{2.24}$$

Next, solve for the maximum values will give the maximum load and these values can be used as a regular value for the previous equation 2.5 mentioned, to calculate the correct amount of stress in the event of a suddenly applied load [15].

It is important to remember that springs are designed to absorb the energy of an impact. The principle of work and energy Equation 2.25 from a kinetic point of view can be taken into consideration as well [7].

$$E = \frac{1}{2}mv^2 \tag{2.25}$$

Where the energy (E) is dependent of the mass (m) and the velocity (v) of the falling object, instead in Equation 2.26, the energy can be determined as half the total load times the deflection of the spring [15].

$$E = \frac{1}{2}F\delta \tag{2.26}$$

It is possible to then use Equation 2.25 and 2.26 to convert them into a more eligible method to calculate either the maximum velocity on which the spring can absorb the energy of the maximum deflection. It is also possible to calculate if the spring can sustain the stress from an impact on a given time.

2.3 Mechanisms of ageing in steel springs

2.3.1 Corrosion

The word corrode is derived from the latin *corrodere* which means to gnaw to pieces [22]. Corrosion is defined as the destruction or deterioration of a material based in its reaction with the environment, practically all environments are corrosive in a certain level [23].

They're different ways to classify corrosion, one method is to divide corrosion in low-temperature and high-temperature corrosion; another is to separate corrosion in oxidation and electrochemical corrosion and a third classification is wet corrosion and dry corrosion [23].

There are three possible reactions a metallic component may present in a corrosive environment, and they are represented in Figure 2.9. The first reaction is immunity; where the material is not affected by the environment and no loss of material is present. The second possibility is called passive, in which a small and thin layer of material is corroded and creates a protective film avoiding further corrosion on the material. In this condition if the film is broken or scratched, further corrosion may be present and more aggressive or rapid corrosion may occur. The third reaction is called active, which led to the lost of material where the metal corrodes and dissolves in the environment. In this last reaction the corroded area does not create any protective

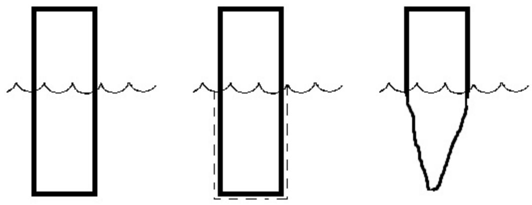

(a) Immune (b) Passive (c) Active

Figure 2.9: Behaviours of metal in an environment [22].

layer and the material disintegrates to expose new material underneath [22].

It is invariably preferred to have an immune response from the material on the environment. It can be achieved with a certain combination of materials and environment conditions, however it is a hard combination to achieve. The passive behaviour can be considered as the second best, although it may have disadvantages, it is still preferable than an active behaviour.

In order to electro-chemical corrosion to appear they are four requirements to complete the process, represented on Figure 2.10. The first two are different elements, which depending on their nobility (Table 2.5) will take place as a cathode or an anode. The anode is where the corrosion will take place while the cathode will not suffer any corrosion or weight loss. The third requirement is a ionic current path, usually the connection is a solution between the first two. The last requirement is when two elements are connected by an electronic path, this will enhance the transfer of electrons causing direct current flow through the corrosion cell [22].

One of the main problems of metallic materials that are exposed to the environment is the process of oxidation. This process alters both chemical and mechanical properties of the corroded material, and eventually leads to a complete failure of the material. The oxidation process is basically a loss of electrons of the material, taken away by the available oxygen in the environment, the reaction between these two will dictate the amount of oxidation that will present on the material [24].

First the oxygen molecules will be absorbed on the metal surface, which then will dissolve in oxygen atoms [25], the oxygen atoms which will be at the surface will create stronger bonds and will allocate themselves in places where they can interact with the most neighbours atoms. This is why some crystallographic faces show more absorption than others [26]. The process of absorption and nucleation are quite complicated and have too many variables from one metal to another. The path that may be expected is the one that presents the least resistance, for example those areas that are already under a strain deformation [27].

Metal ions are attracted to the cathodic surfaces called cations, while the oxygen ions are attracted towards the anode surface and are called anions. The oxidation process can be either by the consequence of ions movement to the outside of the cathodic interface or by the movement of anions to the inside of the metal-oxygen system [22].

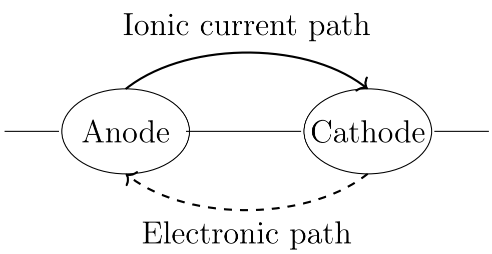

Figure 2.10: Requirements of an electrochemical corrosion cell [22].

It has been established when a metal corrodes at the surface of the material, an anodic site and a cathodic site will generate, these sites can remain permanently, or in some cases there is the possibility these sites will switch. These changes can cause a determined site in the oxidation process at some point can be cathodic and at a different time it can be anodic [27].

If corrosion sites only cover a proportional small area of the material this may lead to a significantly big cathodic surface area, which under this circumstance corrosion sites may become strongly active and create a deep penetration. This kind of attack is known as pitting corrosion, and is a problem for those metals and alloys that have thin protective or resistant films [27].

Atmospheric corrosion is mainly based on two principal variables, humidity and contents of the environment atmosphere, this will establish the quantity of corrosion that can be present at the exposed material. Normally there is a critical amount of humidity that corresponds to condensation condition, after this condition is met the amount of corrosion will be increased considerably. While more polluted the atmosphere is, the more aggressive the condensate film will be [22]. Chloride concentration in the atmosphere tend to initiate localised corrosion, and as a result it will create pitting. Pitting can be significantly deep, reaching total perforation on the material. It is really difficult to generalise the reaction of the metals or alloys in the atmosphere, due to the big variables on condensation and pollutants that may be present at that specific moment [27].

2.3.1.1 Types of corrosion damage

Some of the forms of corrosion are unique, but all of them are interrelated. The most common forms are: uniform, or general attack; galvanic or two metal corrosion; crevice corrosion; selective leaching; erosion corrosion; intergranular corrosion; pitting and stress corrosion [23]. Trans-granular corrosion and corrosion fatigue are not so common forms of corrosion, a representation of these can be found in Figure 2.11.

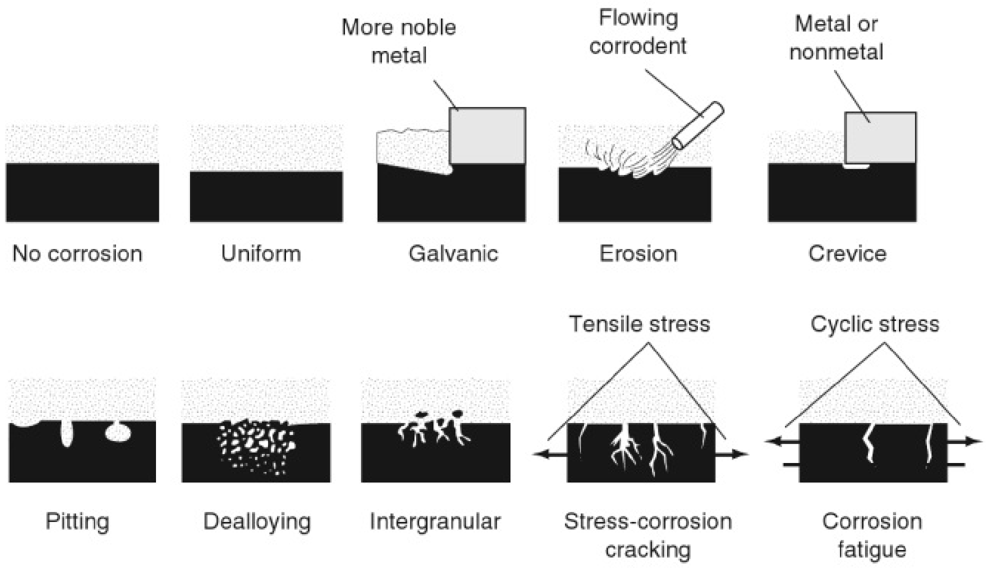

Figure 2.11: Schematics of the common forms of corrosion [22].

The most common failures associated to the corrosion of metallic springs are the stress corrosion cracking (SCC) and the corrosion fatigue (CF), each one with its own set of characteristics and specific circumstances for such failures to occur. A method to catalogued the types of corrosion is presented in Figure 2.12.

Uniform or general attack is the most common type of corrosion, is normally characterised by a chemical or electrochemical reaction that proceeds uniformly over the entire exposed surface or over a large area [23]. A product of this type of corrosion is a red dust commonly known as rust, however the word rust is only reserved for iron elements.

Galvanic corrosion occurs when a metal or alloy is electrically coupled to another metal in the same electrolyte. The difference of potential between the metals create a flow of electrons that causes the less corrosion resistant

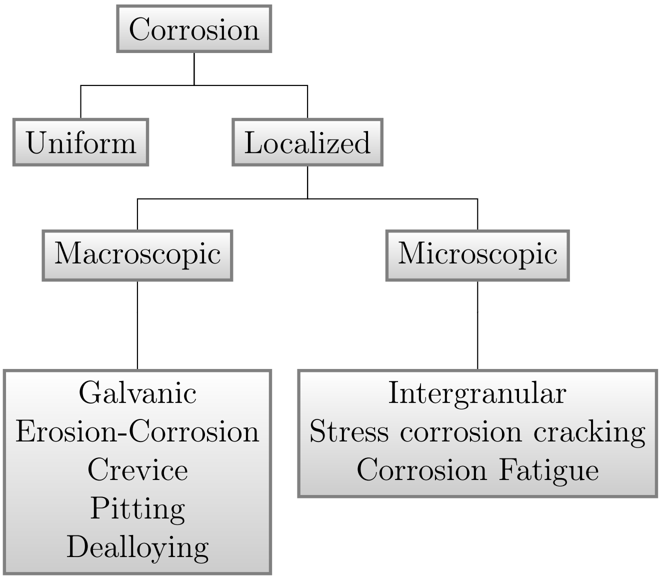

Figure 2.12: Macroscopic versus microscopic forms of localized corrosion [22].

metal to suffer more damage, while the most resistant metal surface becomes cathodic and suffers less or no corrosion [22]. The different combination of metallic elements can vary which will material will respond as cathodic, in Table 2.5 some common metals are listed.

Selective leaching or dealloying occurs when the corrosion affects only one element of the composition which tends to be the most active element of the alloy. It leaves a porous structure behind and therefore the mechanical properties of the material change drastically, frequently losing much of its strength, hardness and ductility [22]. the correct term is selective leaching, however since it only attack specific elements, usually a new term is created such as dezincification (which is the most commonly known process) or decobaltification [23].

Erosion corrosion is the sum of uniform corrosion plus the aggressive removal of material by an abrasive. It depends upon the development of a surface film of some sort (passivity) for resistance to corrosion [23].

Table 2.5: Order or nobility in common elements [15].

Element	**Least Noble (+) Anodic**
Magnesium Zinc Aluminium Cadmium Steel or iron Cast iron Stainless steel (300 series) (active) Hastelloy C Nickel (active) Inconel (active) Hastelloy B Brasses, bronzes Monel Nickel (passive) Inconel (passive) Stainless steel (300 series) (passive) Titanium	
	Most Noble (-) Cathodic

It is an accelerated attack that supersedes the ratios of either a mechanical corrosion or chemical corrosion action by themselves. Two of the most common forms of erosion corrosion are cavitation and fretting corrosion [22].

Crevice corrosion, generally appears inside crevices, holes or gasket surfaces, which are shielded areas on metal surfaces with a stagnant solution causing intensive localised corrosion [23]. A.J.Betts and L.H.Boulton [28] presented a review on the theoretic analysis of how crevice corrosion is generated in smalls areas with reduced oxygen. They presented an analysis on the different kinds of mechanisms that may induce the crevice corrosion, such as deoxygenation-acidification, used extensively by Oldfield and Sutton [29], among others in mathematical modelling. An IR drop depassivisation or potential shift mechanism is emphasised as a crevice control by Pickering [30]. Other mechanism is inclusion dissolution; in this kind of corrosion the attack seems to have isolated pits within the crevice, which later can unite to give the appearance of a more general attack [31]. Other types of mechanisms had been proposed for different alloys [32], in Figure 2.13 it can be seen the diagram of the more important parameters in crevice corrosion. Different test methods to determinate the crevice corrosion resistance of alloys have been reported [33, 34, 35, 36, 37]. Among there it can be found [38, 39], remote crevice assembly [40] and potentiostatic methods [26].

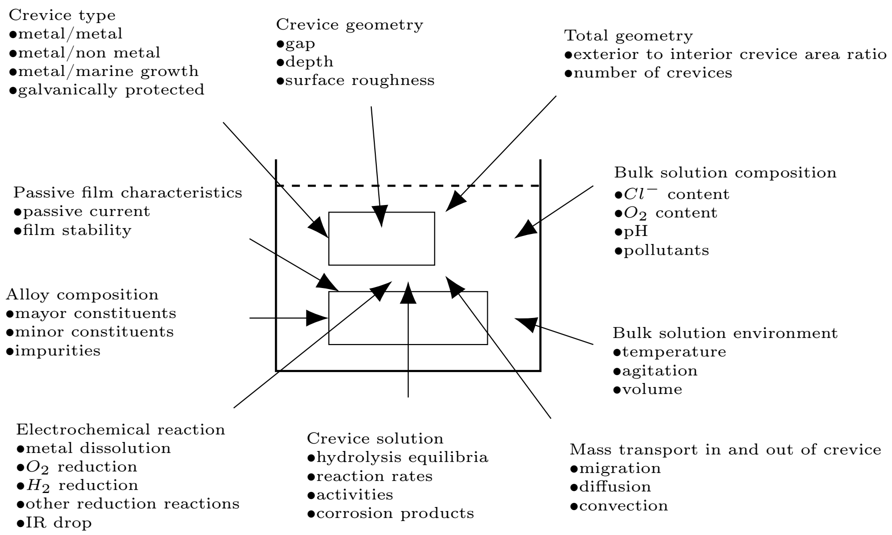

Figure 2.13: Factors thought to be important in crevice corrosion after Oldfield and Sutton [29].

Pitting is the representation of localised corrosion, that produces well defined holes with a determined geometry by micro-structural orientation. The holes can be isolated from each other on the surface, or close enough to resemble a roughened surface. It can cause failure by perforation while producing only a small weight loss on the metal. Every metal or alloy is susceptible to this kind of corrosion. It occurs when one area of a metal becomes anodic while the rest of the surface of the material turns to a cathodic state, or when changes with the corrosive contact and the metal occur. The rate of penetration into the metal by pitting can be from 10 to 100 times faster than that done by general corrosion [22].

It is generally considered that pitting corrosion occurs in three stages: nucleation, metastable growth and stable growth. The metastable growth is a very critical stage of pitting corrosion because only pits that survive this stage become stable growing pits [41].

Pitting is regularly associated with stagnant conditions such as a liquid in a tank or liquid trapped in part of a system, velocity of liquid or increasing velocity often decreases pitting attack [23]. This is due to the fact that after a pit has initiated, the pit initiation site is unstable, and may become inactive if the currents sweep away the locally high concentration of ions that initiated the local attack [22].

Corrosion has an enormous influence on the performance of metallic and steel alloy materials, not only because it changes the chemical properties of the material element but also the physical dimensions. Any change on the geometry of the material will create a new mechanical stress influence on the material. SCC is commonly divided into two phases: the initiation phase, and the crack propagation phase. Several studies had been carried to analyse and determine the crack generation and distribution focused in terms of pitting [42]. As a result of these studies some suggestions have emerged as a possible control on the corrosion appearance and propagation, Figure 2.14.

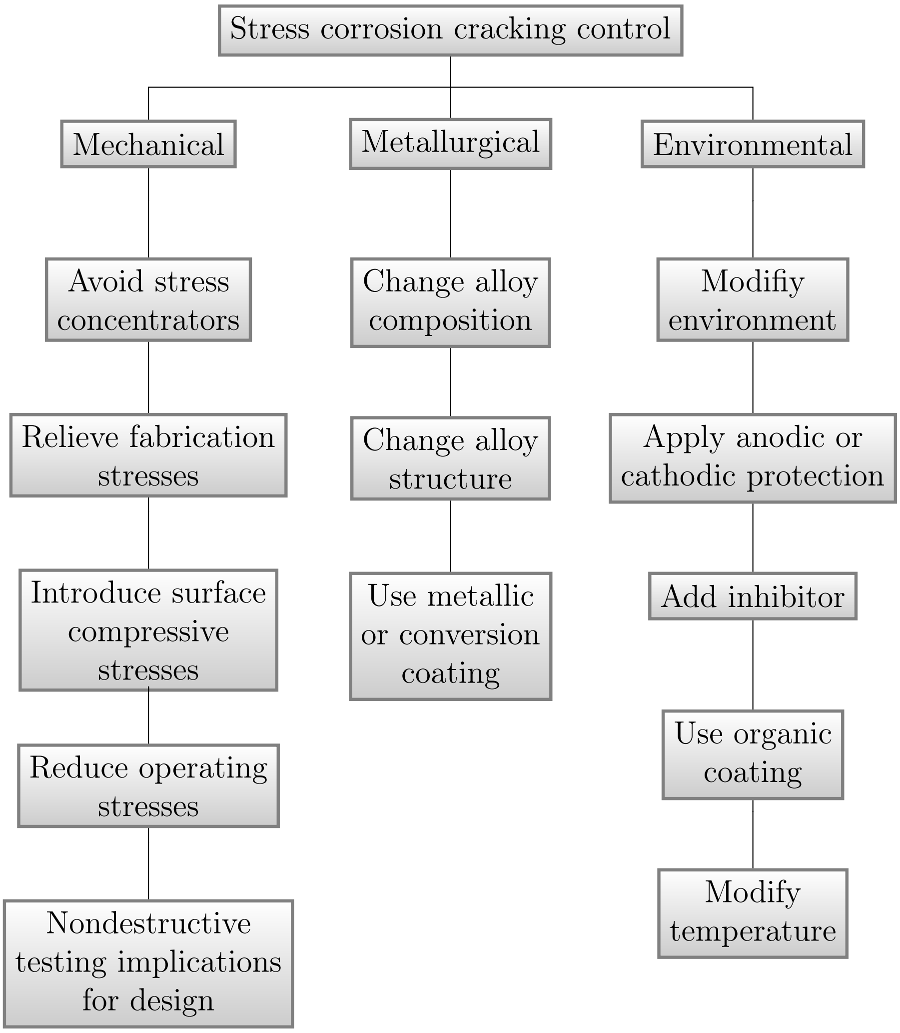

Figure 2.14: Methods used to control SCC [22].

It has been established previously that the starting point for the SCC is the creation of a pit by [43]. Pit formation is still a debate point on the corrosion science investigation, as they are formed from the localised corrosion and accelerated dissolution of the material. The probability of cracking from a pit was described reasonably by the Weibull distribution function [44] (Equation 2.27).

$$F(a) = 1 - exp\left\{ - \left[\frac{a - a_0}{\eta - a_0} \right]^{\beta} \right\} \tag{2.27}$$

Where a_0 is the threshold of the pit size, η is the scale parameter and β is the shape parameter, the value of which reflects the extent to which the probability of crack initiation increases or decreases with time [45]. In order for this situation to continue, the growth rate of the crack shall be greater than the growth rate of the pit [43].

If a metal corrodes, uniform attack tends to be a dominant corrosion process since grain boundaries are frequently only slightly more reactive than the matrix. Under specific set of conditions the grain interface is very reactive and a kind of localised corrosion takes place at the adjacent grain boundary, with little or minimal corrosion on the grains, this is known as Inter-granular failure. The alloy then disintegrates and loses its strength due to the loss of the grain [23].

Inter-granular corrosion may be present due to impurities on the boundary, enrichment of one of the element in the alloy or depletion of one of this elements in the grain boundaries area [23].

The term of corrosion fatigue is used to describe the cracking phenomenon that includes both an initiation and propagation in the material, under the combined actions of cyclic stress, fluctuation and aggressive environment. It depends in the interaction between the mechanical stress and the chemical composition of the material and the surrounding environment variables. It can create failures in shorter stress cycles versus those that are in a more inert environment. This kind of failure produces great range of cracking, from the more fine to the coarse, with few or no branching. It is the main difference between the SCC which usually produces a considerable amount of branching; these cracks are generally filled with dense product of corrosion, as can be seen in figure 2.15. Occasionally this kind of corrosion presents parallel cracks, these are associated with pits, grooves or any other form of stress concentration. Commonly the trans-granular failures are more common in this kind of failure than the inter-granular [22].

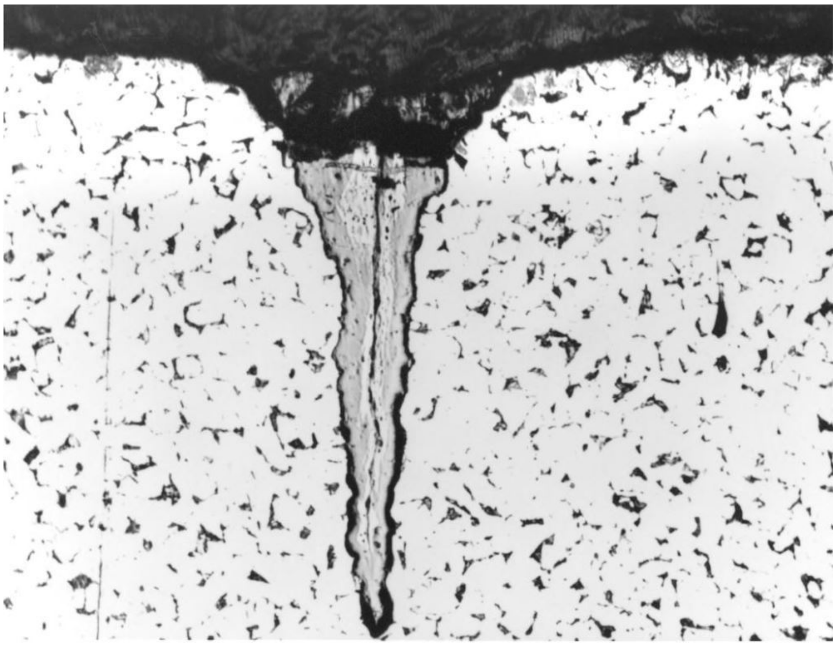

Figure 2.15: Corrosion fatigue cracking filled with corrosion product [22].

2.3.1.2 Previous analysis of types of corrosion

Kondo [43] developed an experiment to measure the pit propagation in a low alloy steel, NiCrMoV (ASTM A294 [46]). It was firstly noted that the corrosion fatigue process was pit growth, crack formation from pit, and crack propagation. Kondo determined the pit size increase following the relation $r \propto t^{\frac{1}{3}}$, where r the pit radius and t is the time. As a result, he established that a crack prediction can be made if the information about corrosion pit growth and the critical pit conditions are known as seen in Figure 2.16. It was reported that a pit was the origin of the fracture for every specimen, and that most pits remained the same size after transitioned to cracks. Another statement was that depending on the cyclic stress, the critical pit condition varied, meaning that the stress level on pit growth accentuate at high values. It was concluded that the fatigue crack propagation from a pit occurs at the point when the fatigue crack growth rate exceeds the pit growth rate [43].

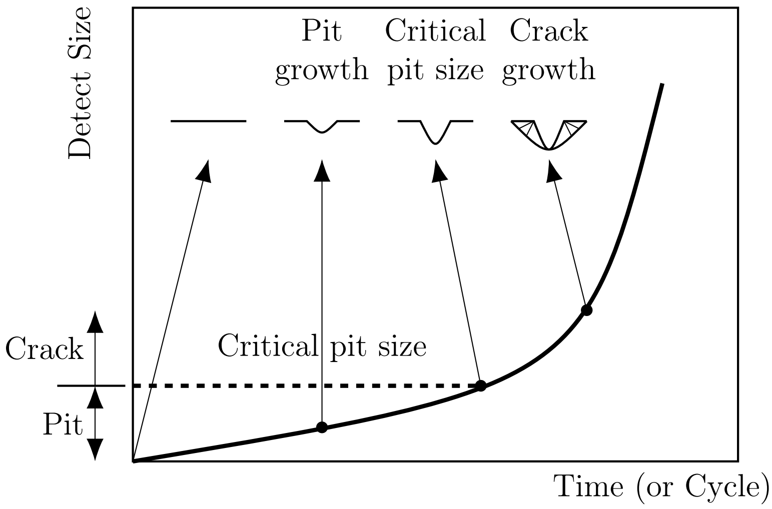

Figure 2.16: Fatigue crack initiation process [43].

Turnbull et al. worked with a turbine disc of 3NiCrMoV steel alloy [46]. The experiment was made to verify the pitting and cracking effect and the propagation of cracks in a controlled environment. It was addressed that doing a simulation of the work load on the material increased the probabilities of corrosion fatigue by including three different set ups of testing. The first set up was with deaerated and high purity water, the second set up with aerated high purity water and the third set up was with aerated water plus 1.5 ppm of chlorine ions (Cl^{-}). The results detailed showed more prominent corrosion for the last set up. After the test regarding the pit diversity, development and evolution of pits into cracks in the material were found. This is an interesting behaviour on which the cracks generally didn't start in the bottom of the pits. It was concluded that using a common methodology in the analysis of the mechanical stress does not result in an adequate representation of the material. The difference in shape and the ratio between the depth and the width of the pits was also recorded [45].

Turnbull et al. [47] Designed a mathematical model in order to predict the propagation and crack generation probability started from corrosion pits. The model initial pit distribution is based on the Weibull distribution [44]. For stable pitting generation and for the pit to crack transition the criteria adopted was using Kondo [43] approach. Basically states the transition that occurs when the pit depth is above the critical value and the crack growth rate is greater than the pit grow rate. The requirement for pit metastable condition is that the pit growth rate has to be greater than a minimum value. The model then was subjected to a stress corrosion test, conducted on a 3NiCrMoV steel disc in an aerated chlorine solution and the results of the test were compared against the model prediction. It was released on the results the model does predict such profiles but to a reduced extent compared with the measurements [47].

Turnbull et al. [48] analised the results obtained by Kondo [43] on the behaviour of corrosion pits and cracks on 3NiCrMoV low alloy steel. They stated that the relationship between pits and cracks is more than a direct formula dependent of the physical characteristics of its elements, as previously stated by Kondo. The stress can be determine and the behaviour described in the generation and propagation of cracks using a finite element model (FEM). Other aspects that should be taken into consideration,are the chemical reactions and weather variables, whose influence reach a significant point in the relationship between crack and pits [48].

Horner et al. [49] compared the corrosion test performed previously by Turnbull et al. [45] by using X-ray micro-tomography [50] as well as scanning electron microscope (SEM). A FEM was used to corroborate the strain generated on the pits using the Von Mises [19] material stress model. The pits were observed and counted, and the evolution to cracks was also under observation in the study. It was noted on previous work by Chastell et al. [51], that pitting susceptibility in 12% CrMoV martensitic stainless steel is strongly dependent on the level of applied stress. In this situation no significant effect appears after loading and based on the X-ray analysis is concluded convincingly that the preferred site for crack initiation is in the pit wall near the mouth of the pit [49].

Suter et al. [52] supported the idea that the combination of sulphur species from the dissolution of manganese sulphide inclusions and chloride within the pit will enhance the electrochemical driving force of pit growth. With chloride at the pit base increasing by virtue of potential gradient, the influence of applied stress on the pitting behaviour was evaluated. The deep inclusions created an active pitting site, while the shallow inclusions only created metastable but not stable pitting. Cracks were also formed even within the shallow inclusions by applied stress [52].

Wang et al. [41] presented an automaton cellular model [53] with Neumann [54] neighbourhood and seven kinds of sites. Only the nearest four neighbours are considered in the model as represented in Figure 2.17. The authors included some rules for the model; electrochemical reactions, based on the combination of two sites a reaction is considered to occur, diffusion of hydrogen ions with Chopard [55] block algorithm adopted, salt film hydrolysis, and mechanoelectrochemical effects based on Gutman [56] model. It was complemented with an FEM, used to study the meta-stable growth of corrosion pits and their transition to material stability. In this case it was used stainless steel under mechanical stress to understand the behaviour and characteristics of the corrosion pit growth. If the material is being exposed to a load, the current density increases against the same object in free state. This gain induces a growth in the centre of the pit, developing its depth and location. When being exposed to a current the generated salts, which are deposited on the inner walls of the pit, engage the process of hydrolysis. The deposition in turn generates new ions which maintain the electrolytic environment and eventually, from having a greater potential difference, generate more corrosion. This process now is in a scale of stable growth, self induced or auto-catalytic generation. On the other hand the material that was free of stress, in these same circumstances, the pit usually re-passivated. All of the simulation results are in close agreement with the experimental observations released [41].

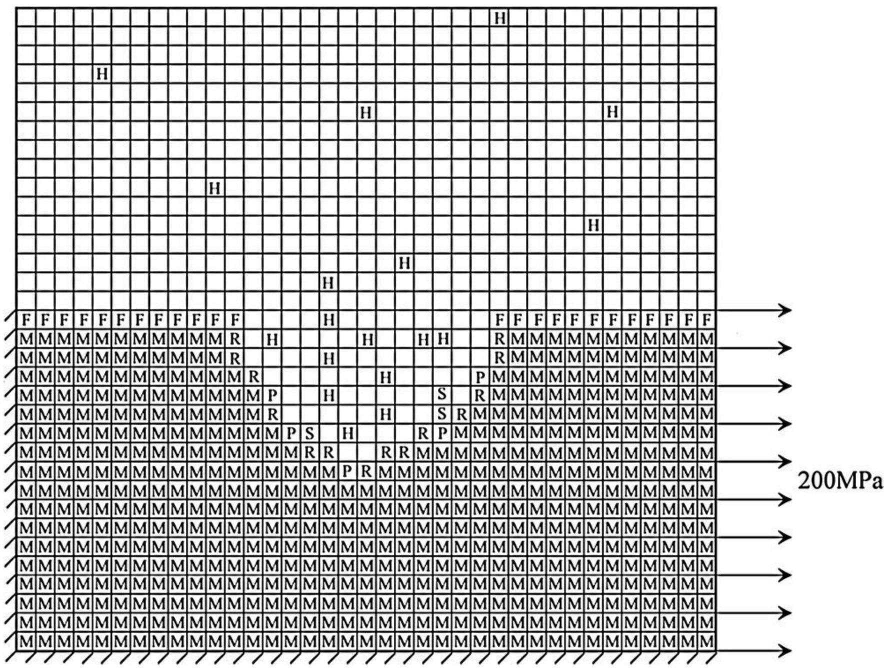

Figure 2.17: Schematic diagram for cellular space [41]

Engelhardt and MacDonald [57] demonstrated how an analogy between the pit growth and the movement of a particle on the material was created. It was suitable as a base for a more general theoretical damage function analysis (DFA), and the unification of deterministic and empirical statistical extreme value statistics (EVS). These were used for predicting the development of localised corrosion. It started from the kinematic characteristics parameters of birth, propagation and re-passivisation of the material. If such values are not available, it can be possible to generate a first model and after first values are calculated, iterate. To maximise accuracy it was recommended to use extreme values of distribution. A comparison is done later with values in function of short periods of time to refine the fidelity of propagation behaviour on the material. This analogy is specially applicable when the external characteristics, such as corrosion potential, temperature, electrolytic composition, are variables with time [57].

Luther and Könke [58] focus their work on a new mathematical approach to the generation of inter-granular relationship inside the models. It was done with the purpose of estimate the behaviour and fatigue conditions in materials with different grain structures. The new model of grain generation, through the use of polycrystalline Voronoi's [59] structures, behaves better in the material characterisation. It also describes the differences that were made to obtain this new distribution of grain area, where the most significant difference is to have a predefined grain size before the generation of the diagram. It allowed to give a more realistic grain size distribution of the material [58].

Jivkov et al. [60] used a FEM to analyse the inter-granular fractures based on the optimisation of the grain geometry. On this specific model the time and kinetic relationship of the crack is not involved, only the appearing and propagation based in the localised stress of the surrounding areas. Transferred through the boundary of the geometry, the model obtained a good correlation between the experimental results published by Gertsman [61]. The model illustrates its capacity to simulate the development of the inter-granular cracks [60].

Luo et al. [62] studied corrosion analysis and pit growth on aluminium alloys, it was found that the inter-granular attack was mainly on grains of high storage energy. The grain that was the preferred to be attacked was located in the boundary, which disclose the growth trough the inter-granular border of such grain [62].

Wenman [63] presented a model that was used to generate a simulation of a stainless steel cylinder, immerse in magnesium chloride, from a mechanical point of view. It was created to estimate the crack network propagation, predict the interactions of the cracks with the stress fields and show the distribution of the stress field during the crack propagation process. The focus on the model was to obtain a typical crack morphology of trans-granular stress corrosion cracking (SCC) in a sample geometry. Based on the initial steps, as pits induced by stress, the model results were compared with experimental samples, to obtain a general agreement between the model and the test. The crack growth was best described by the resolved hydrostatic stress at the crack tip rather than the deviatoric stress concentration [63].

Berger and Kaiser [64] presented the results of an experiment, where springs, made of SiCr alloy steel, were submitted in a fatigue resistance test. The results were gathered and failure was found at a minimum of $12x10^7$ cycles. It was observed that the fatigue limit needed to be deducted a 10% to obtain a value of survival around 90% after the 10^8 cycles. The fatigue limit needed to be decreased almost a 90% to obtain a minimum of 25%

survival rate of the springs after the 10^9 cycles. After 10^8 cycles the failure of the material is likely to be initiated on the inner coil surface instead of the outside surface. After analysing the springs, it was reported that failure will tend to happen at an area with internal dissimilarities, such as inclusions in the material [64].

Rokhlin et al. [65] related the reduction of life cycle in fatigue and the presence of pitting in the material. In this experiment the material used was AA2024-T3 alloy, and was submitted to a determine cyclic load to examine the cracking growth. In the experiment were included previously created pits to simulate real pits under corrosion. The propagation of pits was analysed using a microradiographic method. A three-dimensional fracture mechanical model based on the Paris Power law [66] was created to identify the transition area. A simple empirical relationship was developed to predict fatigue life (Equation 2.28).

$$N_f = N_{th} \left(\frac{d}{h} \right)^{-\frac{3}{4}} \tag{2.28}$$

Where d is the pit depth, h is the sample thickness, and N_{th} is the fatigue life of the sample with a through hole [65].

2.3.2 Surface conditions

The first defence against corrosion of any material is the surface itself. Depending on the material and the circumstance it may behave completely different. The response could be either a catastrophic condition of corrosion or a long span of life. The surface can react to the environment to create a tin layer of protective coating. It also depends on the morphology of the material surface, as it can create more localised points of corrosion, or be resilient to the conditions.

There are several kinds of treatments that can be applied to a material in order to increase its resistance against corrosion. The most common are shot peening and passivisation; the shot peening was firstly introduced by the Associated Spring Corporation to commercial production in 1929 [15].This treatment was originally introduced to increase the maximum stress on the material, Figure 2.18.

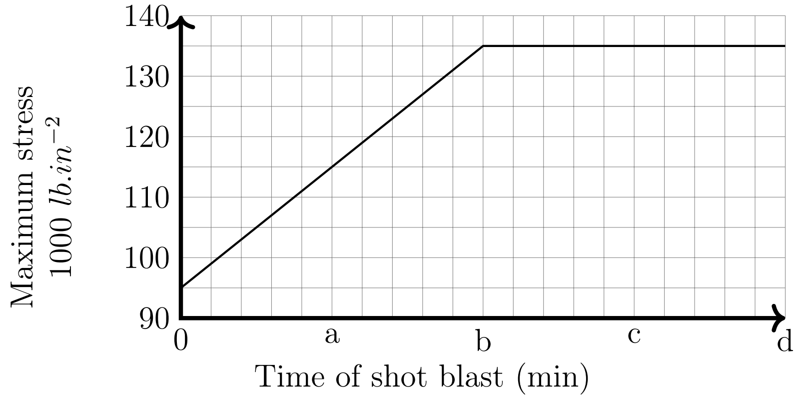

Figure 2.18: Effect of time on shot blasted springs [15].

The shot peening process is a mechanical working process, the results can be affected by heat. If sufficient heat is applied to the spring material after the shot peening process, it will affect the new properties created by the shot peening process. In Figure 2.19 is represented how the performance of the springs can be diminished by the increase of temperature [15].

2.3.2.1 Previous analysis of surface conditions

Aggarwal et al. [67] carried out an experiment to develop a new mathematical model of fatigue failure prediction on materials for a determinate stress and a specific shot peening process time. The model was validated using the results of an additional experimental test. The material used was EN45A,

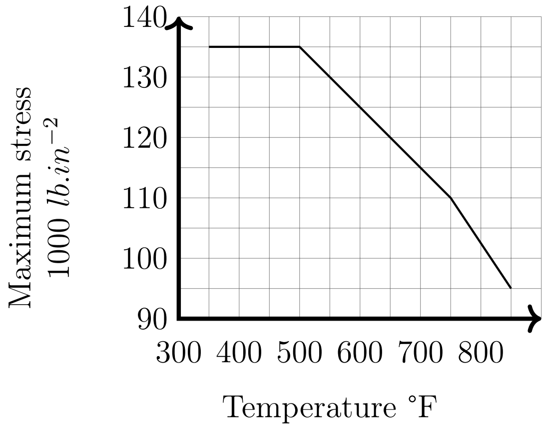

Figure 2.19: Effect of heat on shot peening springs [15]

this material is commonly used on suspension systems for a leaf spring type. The results between the model and the tests were released as significantly representative. The surface treatment was varied to predict the behaviour of the material on a stress load, it presented good predictive results from the model [67].

Zhou et al. [68] presented an analysis of filiform corrosion. This type of corrosion appears in metals that have fine coating layers and is considered a cosmetic form of localised corrosion. In this study the material was aluminium AA5005-H14 in different cleaning stages, as rolled condition, mechanical cleaning and chemical cleaning. The best results against corrosion were reported to be from the samples chemically cleaned. The results were analysed by transmission electron microscope (TEM), SEM, and energy-dispersive x-ray spectroscopy (EDX). It was found that this type of corrosion is controlled by the micro structure near the surface. In the cleaned surfaces the localised corrosion of the substrate results in successive blistering of the overlying coating [68].

Pyttel et al. [69] used three different springs materials (oil hardened and tempered SiCr, SiCrV-alloyed valve spring steel and stainless steel) and performed a fatigue test on each one. The test was to localise the failure after a surface shot-peening treatment. A second shot-peening process was applied to extend the fatigue resistance. The samples with extended treatment did in fact increase the fatigue strength. This action produces a bigger percentage of subsurface failures. It was concluded from this work that the increase on the process is not consistently the best, depending on the material, and overexposure to a treatment is not regularly beneficial [69].

2.3.3 Recurrent damage

The spring industry has used some defence mechanisms against corrosion trying to delay its presence in different materials. Some of these mechanisms are the creation of phosphate layers, dynamic treatment as surface stress relieves, and the addition of polymeric coatings to protect the material against the exposure of the environment. The protection mechanisms used are not sufficient to avoid corrosion even in the most sophisticated metallic springs after the conditions in Figure 2.10 are met.

It is also important to consider the possible damage that can surge from objects that are lose on the road. Pebbles or different kind of debris materials can remove any additional coatings, deform the surface of the material and expose its core. These impacts or external damages will result in a faster corrosion and the external damage can not be controlled.

2.4 Finite element modelling simulation

2.4.1 Previous simulation models

Turnbull et al. [70] presented a FEM of a cylinder model with a pit to evaluate the stress distribution and tension on the near surface. It was in the previous experiment analysis of a low alloy steel turbine disc showed that the crack evolved from the pit, mostly from the mouth or near the pit's mouth, instead of the pit's base as assumed previously by Kondo [43]. The simulation carried two possible scenarios, one was a static pit and the second was a pit growth. In the first scenario, two pits were simulated, one with a hemispherical shape and a second with a bullet shape. The trend for the bullet shape was similar to the hemispherical, however more localised strain was found near the mouth of the bullet shape pit, as seen on Figure 2.20, based on a proof stress of 0.2% yield strain ($\sigma_{0.2}$). In the scenario for the growing pit, the plastic strain was the main focus of approach in the simulation on how the strain would evolved. It was an attempt to recreate the stress relocation, based on the removal of material on the simulation as seen on Figure 2.21. This distribution of stress was also reviewed by Pidaparti and Rao [71]. Based on the information obtained by the simulation it was reported that the plastic strain can be localised on the walls of the pit just below the pit's mouth rather than the pit's base, and after plasticity the stress is redistributed towards the pit's base. This dynamic plastic strain can be considered as a possible factor for determining the transition between a pit to stress corrosion crack [70].

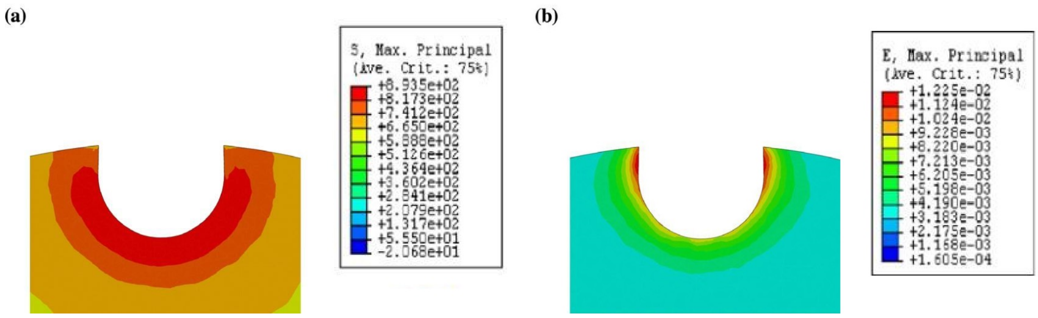

Figure 2.20: Maximum principal stress (a) and maximum principal strain (b) of 500 μm U-shaped pit, applied stress was 90% of $\sigma_{0.2}$ [70]

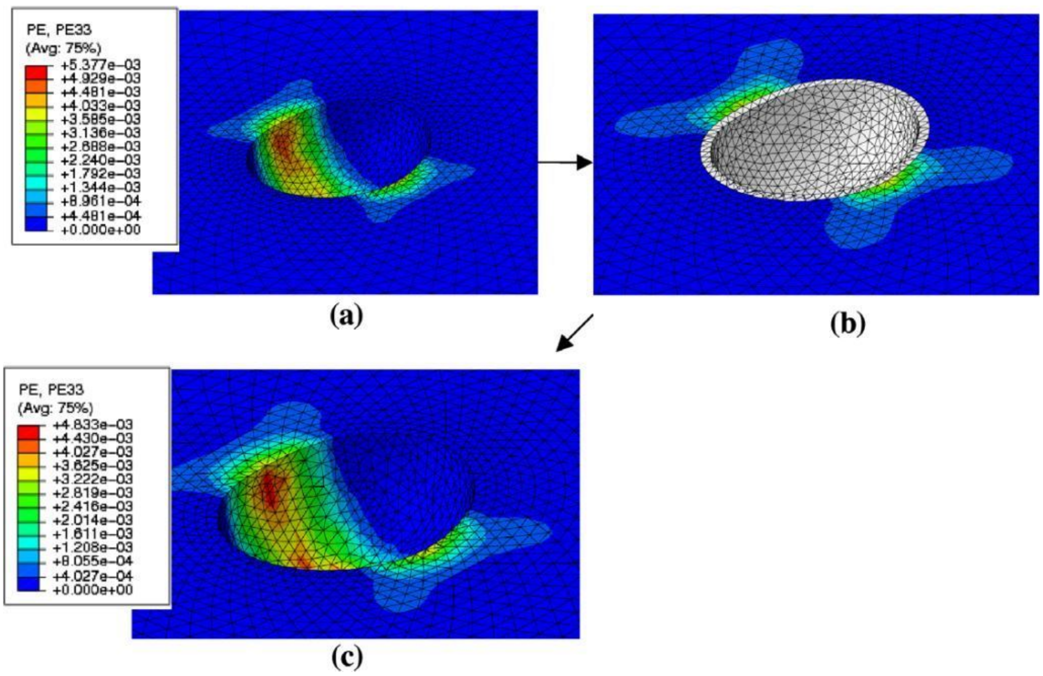

Figure 2.21: Simulation of pit growth by incremental removal of material for a hemi-spherical pit at an applied stress of 90% $\sigma_{0.2}$ only the plastic strain is shown a)initial pit size b)material removed grey zone c)final pit size [70]

Zhao et al. [72] create a finite element analysis (FEA) of cracks and crack generation was performed based on the oxidation of an NiCrAl alloy in this case, subject to a constant load. It was analysed in two situations, vacuum and under rich oxygen atmosphere. It was conclusive in this experiment that the crack is more dependent in the location rather than the wear of oxidation, The material characteristics influence more aggressively than the externally applied load [72].

Zhu et al. [73] analysed a spring that suffered a crack failure. The first coil (inactive) was in contact with the second coil (active). Pit corrosion was founded at the analysed sites. This type of corrosion converted the sites into potential places for the materials failure. The samples were analysed by SEM at the areas where a crack occurred. Metallographic analysis and strength tests were performed to confirm the chemical and grain structure for material 60Si2CrVA [74] were in range. A FEM was develop to represent the clash between these two coils simulating the wear down of the coating. The repetitive clash between the coils damaged the coating, which allowed the corrosion to initiate. The stress created by the clash of the coils in the close ends of the spring resulted in the fatigue crack initiation. Once the initial cracks were formed, the maximum principal tensile stress was the stress that force the crack to propagate, in this case in the direction of 45°of the spring axis [73].

Jivkov et al. [75] used a two-dimensional model to analyse and compare the inter-granular fractures against the previously proposed models using a percolation-type, such as those presented by Palumbo [76], Gertsman [77] and Lehockey [78]. On these models they assumed the grain boundary could be either completely resistant or completely susceptible to SCC. In the model proposed by Jivkov an hexagonal isotropic geometry and two conditions on grain boundaries were used. The first condition can be low energy or high energy, which correspond to the special grain boundaries which are generally accepted as resistant to corrosion. The second condition includes random grain boundaries which are accepted as susceptible to corrosion. The distribution of these boundaries is randomly assigned. The proposed model was checked if it could reproduce the previous percolation models. The set up for the percolation models was stated in an article published by Jivkov [79]. The proposed model has the potential to simulate inter-granular crack propagation in a realistic manner by including the phenomenon of crack bridging. The model also takes into consideration the effects of external load magnitude and the failure properties of susceptible and resistant boundaries [75].

Kumar et al. [80] analysed springs used to keep in position a coke oven producer. The charcoal used in the heating process tends to expand and needs to be maintain as close as possible. This springs had a significantly low life span compared to the calculated design. An unused spring was analysed and compared against an already cracked spring from the oven. There was no difference on the chemical composition of the material, and the grain formation was similar. The heating environment to which the spring was subjected to was not the main cause of failure as a previous theory suggested. Significant particles of sulfur were found on the surface of the cracked spring and pits. These findings lead to the conclusion that the main cause of failure on the springs was the corrosive environment caused by the sulfur material existing on the area, increased by the lost of residual compression stress on the surface of the spring [80].

Prawoto et al. [81] reported the steps for the creation of a FEM and the analysis of some of the possible sources of failure in springs. The different origins could be inclusions on raw material, surface imperfections; caused by improper heat treatment, cold drawing, poor shoot peening, or decarburization. This different kind of imperfections can be catalogued in the manufacturing process. The FEM was focused to determine the local stress distribution around a given defect. Any of these defects were considerably smaller than the complete spring, a sub-modelling technique was put into practice. The software used was ABAQUS version 6.14. Two different configurations of meshing were used, one was the brick element with three dimensional continuum 20 nodes elements (C3D20) and the second one was a quadratic element of three dimensional continuum 10 nodes elements (C3D10). The material properties used for the input on the software were E of 210GPa and ν of 0.3. A simulation was performed with no defects, to use it as comparison against the different defects on next simulation. Four different models were created, each one with different defects. First model had an inclusion, second model was a surface imperfection, a simulated crack. The third model was an attempt to simulate corrosion with a bit of the surface material removed, and the fourth model was a simulation of decarburization, which had a thin layer in the outer surface. The results showed a significant possibility of real threat to create a failure or meaningful reduction of the life cycle of the spring. The author concluded that the integration of the FEM will also help to improve the design of springs [81].

Pidaparti et al. [71] performed a comparison between an experimental process and a FEM. This comparison was about the propagation of stress, induced by cracks which are generated from pits. The material used in this experiment was AA5059, where the samples were exposed in a mixture of elements using the standardised ageing test ASTM G66 [82]. The samples were stimulated at 80°C for up to 100 days. The formed pits were measured with a commercial pit gauge, Starred Pit Gauge, and the average size were estimated using a blister size measurement procedure [83]. The number of pits that appeared was determined and final counting, based on the size was made. The average size and the distance between the pits was also defined. An image model was made using the micrographs taken by SEM and then exported to a surface modelling software Rhinoceros, to create a 3D pitting surface. Some corrections were made on the size and depths of the pits, and then the model was again exported, now to another software, SolidWorks. This software is able to create a 3D model of the corrosion pits based from the 3D images. Finally the model was generated and exported to ANSYS to finalise the FEM and perform the stress analysis. The results showed a range of the specimen sensitisation from 50 days to 74 days, the highest stress levels increased by about 56%. Further increase in the sensitisation time, in the range from 74 to 100 days has very little effect on the stress level was also noted [71].

Del Llano-Vizcaya et al. [84] designed a FEM as a predictive method of a spring failure based on the cycle number. Three different methods of critical plane approach were used, Fatemi–Socie [85], Wang–Brown [86] and Coffin–Manson [87] criteria were the ones selected for this analysis. They were compared between each other and analysed to understand which one provides the best possible result to estimate the fatigue life of the spring.

All the models were compared against an experiment that used a spring material AISI MB high carbon steel. Fatigue tests were performed to obtain the stress against cycle curve at fixed mean stress, (τ_m) of 254.9 MPa. The stress analysis was made in the finite element code ANSYS and the multiaxial fatigue study was made using fatigue software nCode. It was concluded that the critical plane Fatemi–Socie approach gives a good a prediction of fatigue life, while the Wang–Brown overestimates the spring fatigue life and finally the Coffin–Manson model values are lower that those obtained in the experiment [84].

2.5 Concluding remarks

The importance of the properties a material must have, such as torsional yield strength, ultimate tensile strength and corrosion resistance, for the material performance in order to be an appropriate candidate for a spring are mentioned. It is shown how to calculate the spring rate and how to obtain the stress value the material is subjected to under a specific load.

It is remarked the geometry and the spring material are directly related, and any modification on either one variable will cause a change in the performance.

It was mentioned which are the characteristics that generate the different types of corrosion and how the environment plays an important role on every different mechanism.

It is stated that small imperfections can lead to local corrosion sites. Irregularities that break with the homogeneity of the surface on the material tend to a faster initiation of corrosion. These irregularities can be caused either by defects on the material of flaws in the manufacturing process. If the imperfections on the surface are caused from the operation of the spring it still enhances the corrosion process.

Significant attempts had been done to obtain a more accurate prediction of a spring life performance. All these input have created a more complex and reliable simulation of the spring. However it is still not possible to obtain a general model that can exactly predict the relationship between load, performance, corrosion.

Chapter 3

Analysis of metallic spring

3.1 Introduction

In this chapter the microstructural analysis of the spring material is presented. The samples are from the spring material 54SiCr6 [88], which is broadly used by the spring automotive industry. During the manufacturing process a phosphate layer and a final organic coating are used as a defence mechanism against corrosion. The first specimen analysed was a new or unused spring taken from the production assembly line. The second specimen used was a spring that had been subjected to an accelerated ageing test and presented corrosion. The importance to analyse the difference between these two specimens is to identify the type or mechanisms of corrosion. The purpose is to compare the two springs and observe the difference that could exist on the material and the response of the spring under the effects of corrosion.

3.2 Metallography

Metallography is the study of a materials microstructure. Analysis of a materials microstructure helps to understand how the material has been processed and is therefore a critical step for determining product reliability and for determining why a material failed [89]. The basic steps for proper metallographic specimen preparation include: documentation, sectioning and cutting, mounting, planar grinding, rough polishing, final polishing, etching, microscopic analysis, and hardness testing [89]. For the specimen preparation all the steps were carried out except the hardness testing. The material used is widely documented, and it should comply with the requirements listed on the standards of material properties such as BS EN 10080:2002 [90] or ASTM A401 [88].

A new spring and an aged spring were received to perform the analysis and make a comparison between the microstructure and the corrosion behaviour. The first analysis was done with the new spring. The spring was the one used in the suspension system of the rear of the vehicle. All the springs were reported to be made from the same material. The second spring was submitted to an accelerated ageing test. This test is released to be a representative wear and environmental attack for an estimate of 60,000 kms of regular use.

3.2.1 Procedure

All the samples were subjected to the same procedure and finish quality to analyse them. All the steps were replicated on to minimise the difference that could be created on the material to obtain a more accurate comparison.

3.2.1.1 Labelling

The springs are right hand spring and they were marked following the same conditions. It was decided to sample the spring of different locations for the purpose of verifying whether degradation occurs in the same magnitude with respect to the position of the spring. From the upper view, as if it was an isometric model perspective, the start of the material spring was placed on the 12 o'clock position and marked. The second mark was made at a 3 o'clock position, the third mark was made on a 6 o'clock position and the fourth one was on the 9 o'clock position. In Figure 3.1 the letter lambda (λ) represents the location of the marks made on the spring. Each location marked was made following this pattern through all the spring coils giving 32 marks in total (Figure 3.2). A segment between two marks was designated as segment, and they were labeled starting on the top part with number 1 between the first 12 o'clock position and the 3 o'clock position. Following the material natural curvature for the next segment label and again for the complete spring having a total of 31 segments. This help to identify the location of the samples as they indicate the position they had on the spring previously to the cutting.

3.2.1.2 Cutting

The equipment used to cut the samples were a bank saw; used to obtain more manageable pieces, and a disc saw; to make more accurate cuts of

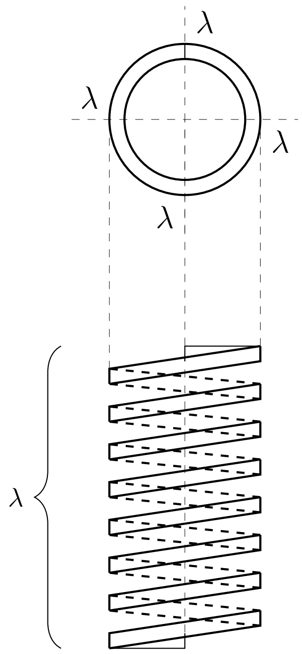

Figure 3.1: Label diagram

the segments as shown in figure 3.4. The next step was use a disc blade of aluminium oxide for a precise cut and finally obtain a thin cross section slice. The equipment used was a Powermet I disc blade saw, with a feed rate of 50% speed to avoid overheating, and a pressure of 70 lbf/in^2 in the thrust cut. Cooling liquid was used to maintain temperature in acceptable levels, as high temperature may expose the material to a change on its structure and change its properties. A cutting disc of aluminium oxide which was certified for materials with a hardness in the range of 300-500 HV was used for the cross sectional cuts.

3.2.1.3 Grinding

A polishing machine (PRESI Mecapol 260) was used to remove any bur left on the samples by the disc blade saw and obtain the finish surface for analysis. The machine was set up at 240 revolutions per minute (rpm) and several sand papers were used. The first sand paper used was a 160 μm grain size followed by 180,400,600,800,1200 μm grain size respectively. The last sand paper was 2400/400, which is considered as a polishing paper. Finally it was used a polishing cloth and paste of 6 microns and 3 microns until all marks left were no longer visible and had a mirror-polished type finish. Every time the sand paper used was changed, the sample was rotated 90°in order to remove any impurity left by the previous sand paper as mentioned in most of the metallography procedures [89].

3.2.1.4 Mounting

The majority of metallographic specimen mounting is done by encapsulating the specimen into a compression mounting compound (thermosets-phenolics, epoxies, diallyl phthalates or thermoplastics-acrylics), casting into ambient castable mounting resins (acrylic resins, epoxy resins, and polyester resins), and gluing with thermoplastic glues [89].

The mounting operation accomplishes three important functions:

- Protects the specimen edge and maintains the integrity of a materials surface features.
- Fills voids in porous materials .
- Improves handling of irregular shaped samples, especially for automated specimen preparation.

Samples were mounted on thermosetting polymer, also known as thermoset conductive resin. A stainless steel strip was placed around the sample previous to mounting in order to increase the electron conductivity on the sample and improve visualization when using SEM.

3.2.1.5 Scanning electron microscopy

The scanning electron microscope consists of an electron gun and a series of electromagnetic lenses and apertures. The electron beam emitted from an electron gun is condensed to a fine probe of surface scanning. An image is formed by a focused electron beam that scans over the surface area of a specimen. One of the most important features of this microscope is the three-dimensional appearance of its images (micrographs) because of the large depth of field. With SEM, chemical information from a specimen can be obtained equipping the microscope with various techniques, like EDX. The acceleration voltage for generating an electron beam is in the range of 1-40 kilo Volts (kV) [91].

The equipment used was a Zeiss EVO 50 SEM equipped with EDX variable pressure capacity using an acceleration voltage of 10kV.

3.3 Sample preparation

3.3.1 Labelling

The new spring was marked as previously mentioned and the label that was given to the samples was based on the segment number the samples were taken from. In Figure 3.2 can be seen how the marks were applied to one of the coils of the spring.

3.3.2 Cutting

The first cut made was in the middle of the spring to have two parts, upper and lower as in Figure 3.3. This was done to give more manoeuvrability and simplify the movements to allow the cuts for the segments. Both upper and

Figure 3.2: Spring showing marked areas for sample cutting

lower part comprehended of 4 coils which give a more equivalent separation on the samples.

Figure 3.3: Side spring view of the lower part, with mark for segments cut areas and numbered to identify location of samples

The upper part was the first part that had the segments cut out. The cuts were done continually with the blade saw. As a result they were 17 segments obtained, as shown on figure 3.4. The next step was to cut from the segments an appropriate sample size, this was done with the blade saw disc.

Figure 3.4: Segments obtained from the lower part of the spring.

The sample size were cut to maintain a thickness of about 5 mm. This thickness was selected to keep a rather flat sample of the material.

3.3.3 Scanning electron microscopy

3.3.3.1 New spring

The samples were chosen from different coils and areas of the spring. It was desired to obtain a more general description of the spring rather than a specific location. The first test sample placed on the SEM equipment was quickly charged electrically, specifically in the coating area. A method to avoid this charge was used, and the images were then possible to be acquired. This method is the addition of a silver painting and create a circuit that grounds the sample. It was identified the upper, lower, inside and outside position of the sample area, as shown on figure 3.5 to review any possible difference of the coating structure or thickness.

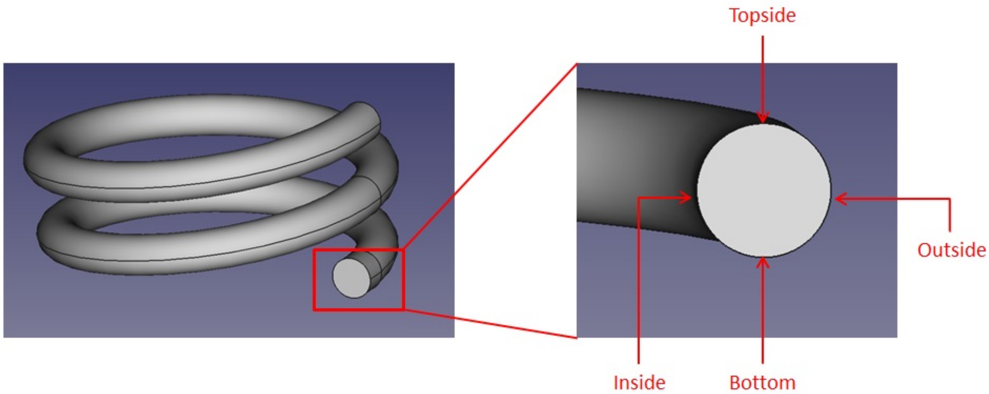

Figure 3.5: Positions of sample cross section in spring wire diagram

3.3.3.2 Aged spring

The aged spring was previously exposed to an accelerated ageing process, designed to simulate the conditions the spring will have to endure. The ageing test can be summarised in the following points:

- Temperature of 45-50 ± 0.4 ℃ at constant settings.
- Relative humidity of 50-95 ± 2% at constant settings.
- Salt spray passage, salt solution used in is 0.5 ± 0.05% sodium chloride, a high-speed splash effect generated at different heights of the vehicle.
- Dust track, a portion of track is covered with crushed granite which generate dust that settles over the dampened vehicle.
- Stone pecking road, a portion of track is covered with gravel laid, simulate stone chipping.

This ageing test was run for a 12 week period with rotation on tracks and driving conditions while the vehicle was under observation for the complete period. After the test was concluded a mechanical compression test were made to the spring.

3.3.4 Results

3.3.4.1 Material composition

To confirm the alloy comply the requirements of material composition an EDX analysis was performed on the samples. An analysis was made at the center of the samples and near the interphase between the coating and the metallic substrate. These regions were selected to confirm any possible difference in composition across the diameter of the wire. Material composition was found for both new spring (Figure 3.6a) and aged spring (Figure 3.7a) to be within the alloy compound listed by ASTM [88] (Table 3.1). However due to the nature of the equipment that performed the analysis, not all the elements could be reported on every sample, or the magnitude of all elements could be quantified correctly. This analysis was more focused into validate the presence of the elements and to find any impurities on the selected samples.

Table 3.1: Material composition of material ASTM 401 [88]

Carbon	Chrome	Silica	Manganese	Phosphor	Sulphur
0.51-0.59	0.50-0.80	1.20-1.60	0.50-0.80	0.025	0.025

A phosphorous layer between the metallic substrate and the coating was found on one of the samples (Figure 3.6b). This layer is part of the manufacturing process and the debonding of the coating could be a result of the grinding and polishing process as can be seen in the micrograph 3.8f.

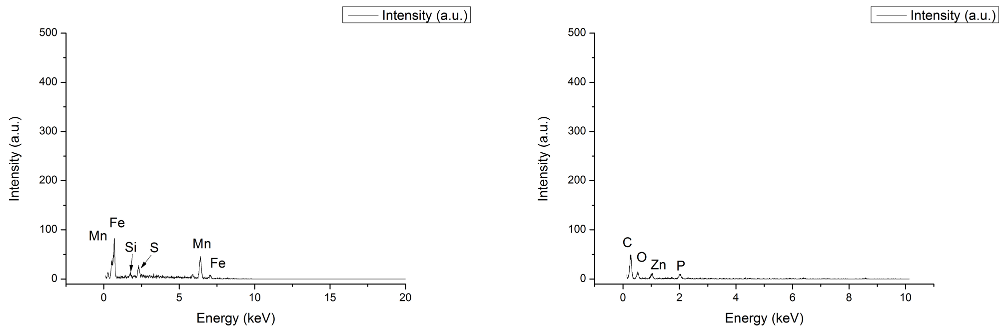

(a) EDX of matrix in new spring

(b) Phosphorous layer between organic coating and metallic subtract

Figure 3.6: EDX values of compounds for new spring and phosphorous layer

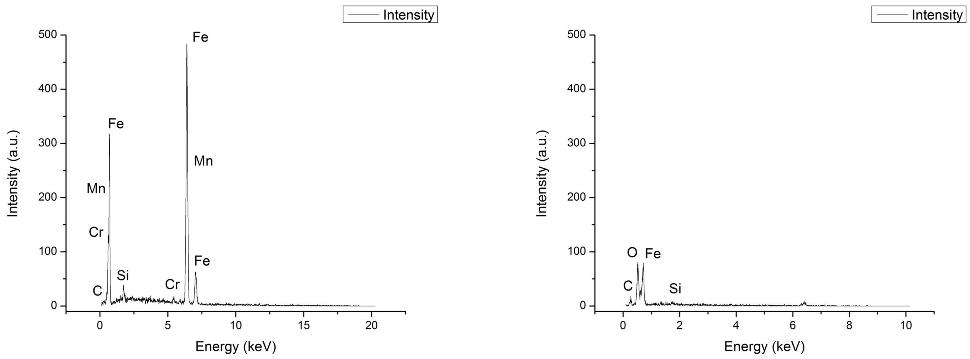

(a) EDX of matrix in aged spring

(b) EDX of corrosion product on aged spring

Figure 3.7: EDX values of compounds for aged spring

3.3.4.2 New spring

In figure 3.8 it is shown SEM micrographs of the cross section of the new spring sample. Micrographs 3.8a and 3.8c show a uniform coating. Micrograph 3.8b shows how part of the coating has been separated from the metallic substrate. This is believed to be caused mostly due to the difference between the materials toughness. It is difficult to maintain both materials bonded together during polishing without damaging the softer material, which in this case is the organic coating. The coating suffers not only the wear from the sandpaper but also blur from the metal. Any debris can damage part of the coating and the bonding between this two materials.

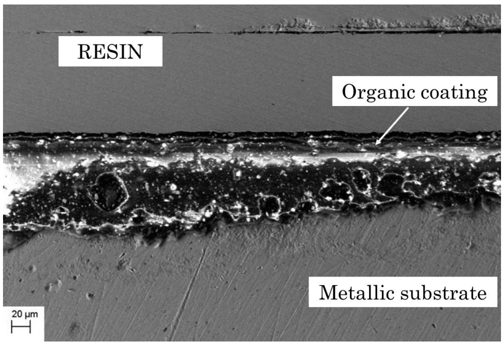

(a) Cross section SEM micrograph of spring sample

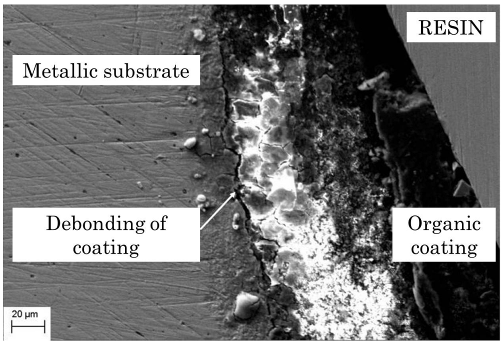

(b) SEM micrograph of loosen coating material from the metallic material

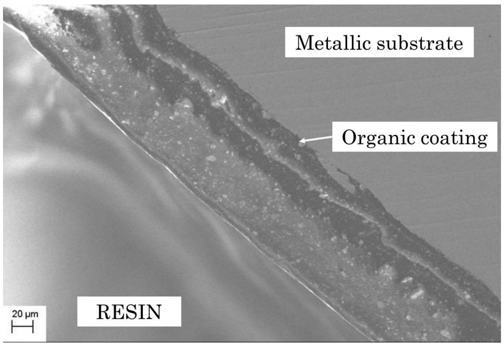

(c) SEM micrograph of continuity of coating material on wire

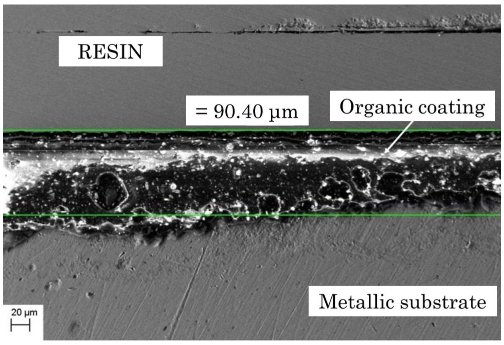

(d) SEM micrograph of sample coating thickness

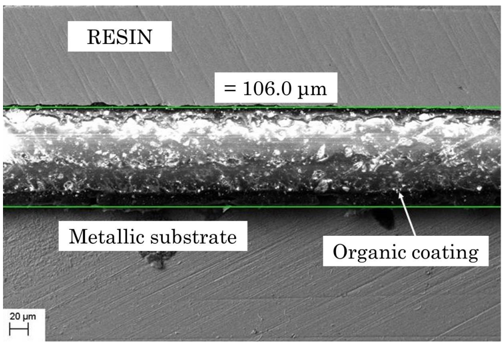

(e) SEM micrograph of sample coating thickness

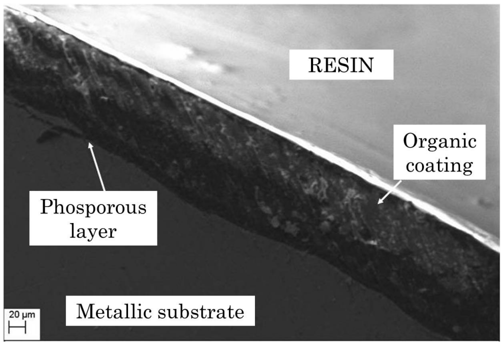

(f) SEM micrograph of phosphorous layer

Figure 3.8: SEM micrographs of cross section of different new spring samples

The coating thickness ranges between 90 and 120 μm. Example of these measurements are in micrograph 3.8d and micrograph 3.8e. It was observed as a general trend through the spring, that the thicker layer of the coating was located on the inner section of the core spring wire. The thinnest coating was on the upper section of the spring wire sample. Examples of the coating measurements are in Figure 3.9 and visual representations of these locations are in Figure 3.5.

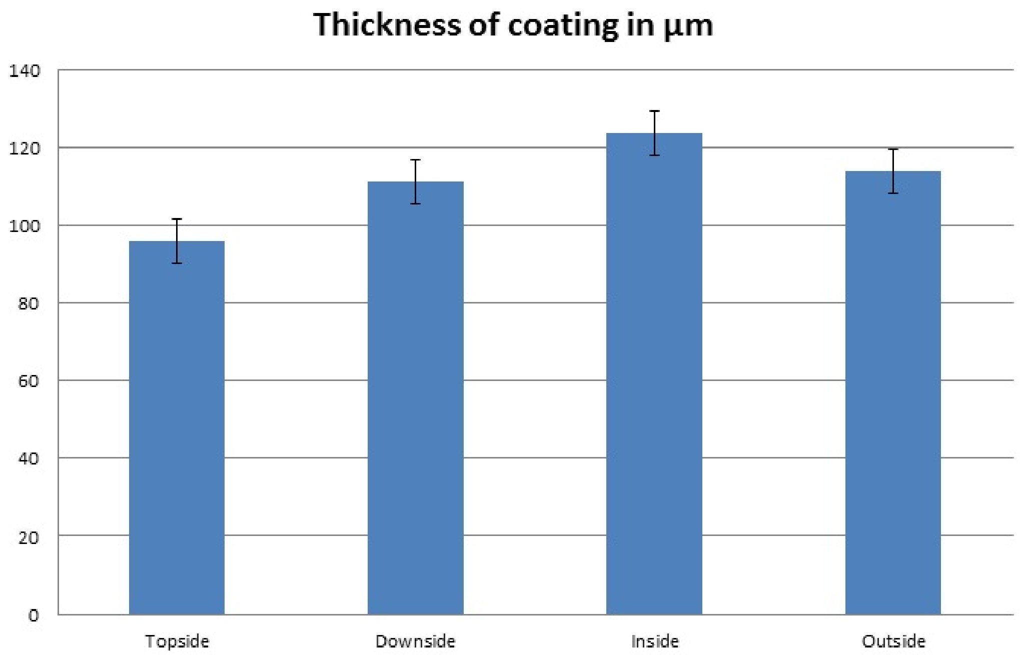

Figure 3.9: Thickness of coating layer (μm) on 34 different samples, with standard deviation error (σ).

3.3.4.3 Aged spring

The corrosion behaviour of the aged spring is presented in micrograph 3.10a and in micrograph 3.10b the presence of pitting, and crevice corrosion is observable. Micrograph 3.10c shows how the coating has been left intact but the metallic surface already has been corroded. At this moment corrosion is expanding and removing the bonding between the coating and the metallic material. In micrograph 3.10d is possible to see a more advance stage of this process. Corrosion had reduced the overall diameter of the cross section circular wire by 2 mm in this particular area. The coating has been broken and now exist a direct contact between the metallic substrate and the environment.

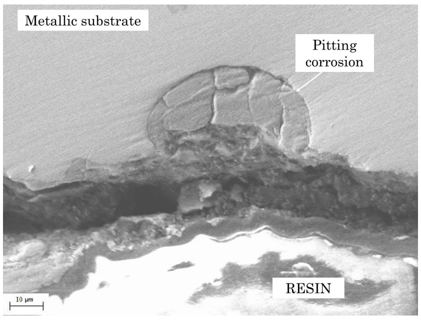

(a) Pitting corrosion site located on the aged spring sample

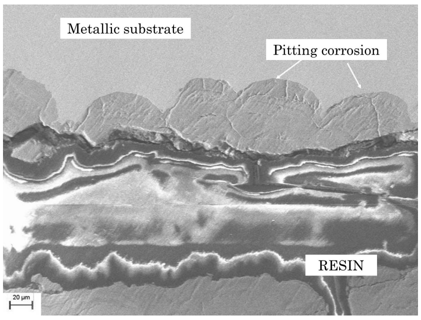

(b) Pitting corrosion site located on the aged spring sample

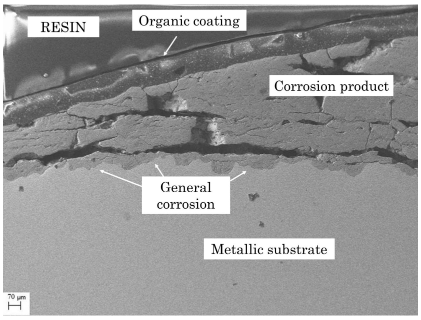

(c) Pitting corrosion propagation

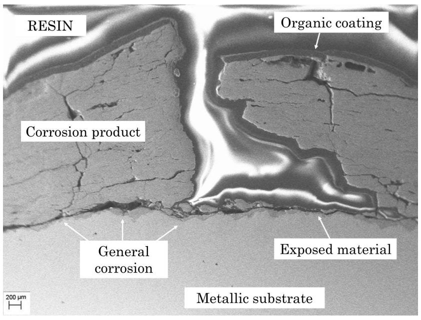

(d) Corrosion remove 2 millimeters of spring wire diameter

Figure 3.10: SEM micrographs of cross section of different aged spring samples

3.4 Discussion

The main information obtained from the analysis of the samples is that the corrosion mechanism does follow the behaviour of theoretical crevice corrosion and general corrosion mechanisms. Corrosion occurs as a general trend across the spring wire rather than a localize corrosion. It reaches the metallic material through the coating by the sites where this has been wear down, chipped, or punctured. This can be caused either by foreign materials, wear down from clash of the coils or even a bad manufacturing process. Once the corrosion mechanism has started, it uses the same coating as part of a crevice mechanism and it expands through the material. This can be seen in micrograph 3.10d. The exposure of more metallic material and removal of the spring coating from the inside can happen in later stages of corrosion.

The stress-corrosion cracking and corrosion fatigue were not observed in the samples. A possible explanation is that the induced ageing corrosion test does not give enough time for this kind of corrosion to appear, since it is not a normal exposition and the spring was not subjected to severe stress for enough time. It is possible to assume this kind of corrosion may appear in a latter stage of the life cycle of the spring. This effect enhance of corrosion resulting in a autocatalytic process of corrosion in the spring.

3.5 Concluding remarks

The methodology, steps involved and what characteristics were taken into consideration for the procurement of the samples was mentioned and explained.

The comparison between the new and the aged spring confirmed the material composition to be within the standards for both springs, and the corrosion theory corroborate with the micrographics obtained from the samples.

It was possible to observe the mechanisms of corrosion on the aged spring after the accelerated test it was submitted to. The information obtained about the spring degradation was used to generate an approximated geometric model in a computer aid design (CAD) software (Section 4.2.1.1).

The justification for the model variations were based on the deviations of the spring subjected to corrosion. Such model will help understand the change in performance of an aged spring due to corrosion.

Chapter 4

Finite element modelling

4.1 Introduction

Finite element modelling (FEM) can simulate the behaviour of the spring under any preset loading conditions previously set up, to visualise the performance. This methodology has been widely adopted due to the good results the available software has provided. It is now possible to generate accurate solutions and the use of simulation helps to visualise the material response. Simulations allow the user to visualise the effects in a more graphic environment. For this work a conical spring with plain end type geometry was used. The analysis and performance of the spring, can be simplified by having this set up geometry on the end type. This analysis was made with the purpose of review the behaviour of the springs under loading and compare the performance of a new spring versus a corroded spring.

4.2 Finite element analysis

Around 1940 solution to an elastic continuum problem was presented. It is not exactly recognised in which precise moment the finite element analysis was born. It appears that Clough [92] was the first to coin the term, finite element, which is implicit in the direct use of the standard methodology applicable to discrete systems [93].

FEM started to be used to perform a discrete analysis of a studied material. It was meant to take a specific shape or figure and then broke it down in multiple elements. These elements are the minimal representation of the material that still behave with the same mechanical properties measured by mechanical tests. A mathematical approximation generates an infinitesimal amount of these elements, this leads to differential equations to solve an infinity number of these elements. This array or system its called continuum, and after the elements have been located inside the continuum, it is possible to analyse them. The next step is to take all the elements and regenerate the shape with the sum of the elements given as result of the behaviour analysis of the material under such circumstance [93].

Since the beginning of this methodology there have been differences between the approaches that should be used to the discretization of the continuum. The mathematicians generated general techniques applicable directly to the differential equations that were governing the problem [94, 95, 96]. On the other hand the engineers, specifically in the solids mechanics area, such as McHenry [97], Hrenikoff [98], Newmark [99], and Southwell [100], tackle the problem in a more intuitive way by creating analogies between the real discrete elements and a finite portions of a continuum domain.

Starting on 1960, such division between the mathematicians and the engineers was no longer significantly existent thanks to the great progress done in this area. The computers, the expediting of the calculation for the elements and the integration and manipulation of results in the continuum, allow a better visual comprehension.

There are two important properties to disclose in the finite element method, the boundary conditions, and the constructions of equations from the element of the global structure. The concept of the finite element method differs significantly from the analytic method as a result of this two properties. In the conventional analysis a problem must determinate the initial condition prior to the problem analysis, which means changing the conditions and repeat the complete process of the problem, for a new solution. In the finite element method only the mathematical expression, representative of the mechanical properties of the structure in the study are determined prior to the analysis. If the initial condition of analysis is modified, the new solution is more achievable. This method suppose that the elastic body is an assembly of elastic components, and in the method where the domain of the analysis is divided in a limited number of sub-domains, the global stiffness is mechanically constructed by combining the properties of the elements of such sub-domains. In Table 4.1 the analytic steps of the finite element method are presented. A structure built with the combination of elastic components is referred to a structure of components [16]. If the problem changes only step 3 need to be modified to satisfy the new conditions and obtain a new result.

In continuum dynamics a common perspective is necessary regardless of the material or kind of object subjected to study. The object is recognised based on two different points of view. The first one is the dynamic point of view which involves stress, body force and surface force. The second is the geometric point of view which includes strain and displacement. The

Step	Component Structure
1	Disassemble into each component Find each spring constant
2	Join components Find composite spring constant
3	Give boundary conditions
4	Solve equation

Table 4.1: Steps for a structure to solve the problem with different boundary conditions [16].

continuum borders the outside of the domain through a boundary, as long as the continuum has a limited domain. It is natural to assume that any involvement of the continuum with the outside of the domain should occur on the boundary. As the continuum is described by a mechanic quantity and a geometric one, there is a mechanical limit condition and a geometric limit condition for the continuum [16].

4.2.1 Simulation properties

This section illustrate how the spring model was discretized and which were the initial conditions. It mentios the boundary conditions and the reasons to perform the simulation under these circumstances. The software selected was commercial software ABAQUS. The three-dimensional object was imported from the spring CAD, represented in figure 4.1.

4.2.1.1 Geometry

The geometry selected for the FEM was a right hand conical shape of eight coils with no end type modifications. The mean diameter of the spring was 120 mm, the pitch was 30 mm, with a height of 240 mm. It had 5 degrees of aperture and the wire diameter was 16 mm. When importing the CAD all the parts of the object were integrated in a single model. This was done to avoid any discontinuity that could be produced from the generation of the solid in the CAD. The imported part was designated as a three-dimensional object, with the possibility to deform. Solid regions were merged into one single piece to maintain the integrity of the analysis.

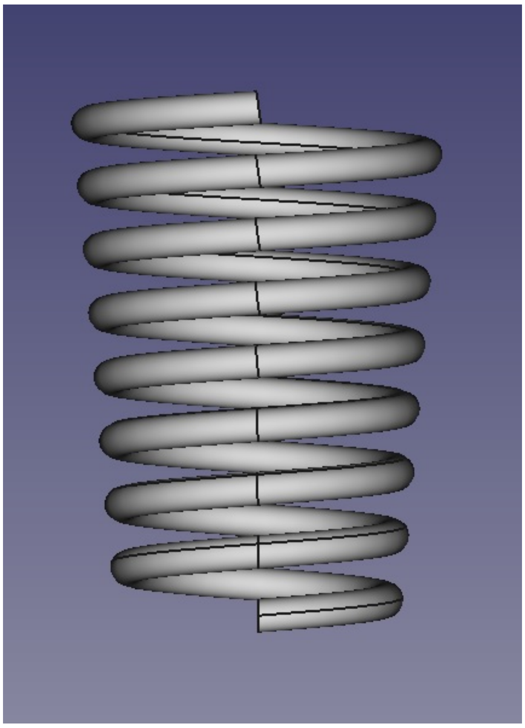

Figure 4.1: CAD generated for spring geometry

4.2.1.2 Material properties

The material mechanical properties defined to carry out the FEM are presented on table 4.2 , based on the information stated on different sources [101, 9, 88]. These values were used in Equation 2.3 to calculate ν. This information was introduced to the software ABAQUS as the material mechanical properties to simulate the performance of the material under specific circumstance. The object was created as an homogeneous solid with the material mechanical properties previously stated.

Table 4.2: Material mechanical properties used in FEM simulation.

Properties	**Values**
Density (ρ)	7850 $\frac{kg}{m^3}$
Young modulus (E)	$206x10^9$ Pa
Torsion modulus(G)	$78.5x10^9$ Pa
Poisson ratio (ν)	0.3121
Yield strength	$1680x10^6$Pa

The objective of these simulations was to obtain a general idea response of a simplified CAD spring behaviour. This behaviour was compared against other simulation of a spring with geometry modifications, based on the material samples examined previously for the samples corroded.

4.2.1.3 Assembly

An assembly of the spring in ABAQUS software was created. The object was rotated and the position adjusted to locate it at a most suitable orientation as shown in Figure 4.2. The next step was to create a procedure in ABAQUS software as a general type, with the condition of general static. The geometrical non-linearity condition was included, in the event of deformation when doing the analysis was present. An automatic stabilization, specified by dissipated diffraction energy was also included in the simulation keeping the default values in the software. The maximum number of increments on the simulation was changed to 10 000, and the increment size was set 0,01 as initial. An automatic size of increment was set as a minimum of $1x10^{-8}$.

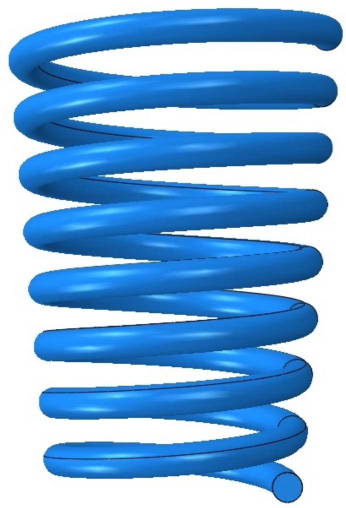

Figure 4.2: Assembly of the spring.

4.2.1.4 Interactions

The coils of the spring were set to act as an independent surface. This did not allow any of the adjacent coils to superimpose. Each coil was selected and given the properties of contact to contact surface. This condition was only applied if the coils did get into collision and avoid any overlap. The ABAQUS software does not take into consideration any contact between surface unless is clearly specified.

4.2.1.5 Boundary conditions

The lower coil was selected and given a pinned condition, (Figure 4.3) which means that it will maintain its position regardless of any acting force on it. It still had the ability of rotation, to simulate the natural twist the spring has to make when it changes in height. This allowed to simulate the spring with a perfect fit on the seat, the seat is the part in which the spring is located in the suspension system, as if the spring would not have any degree of slippage. This may not actually be a real condition, but in order to facilitate the simulation this variable was left outside the criteria of analysis.

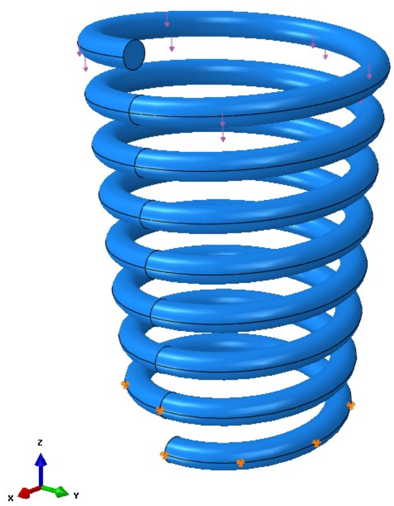

Figure 4.3: Load applied on top coil, bottom coil pinned.

On the other end, the top coil of the spring, the load application was distributed along the first coil simulating a perfect fit with the seat, as it can be observed in Figure 4.3. Only the material response to a static force was considered in the scope. This configuration was chosen to simulate the load that came from the vehicle while it remained motionless. The spring was also restricted to have only movement in the desired axis. The displacement of the spring was restricted to only the longitudinal direction, to avoid possible alteration to the force magnitude by the spring position. The calculated load simulated the weight of a vehicle distributed along the 4 springs, and the proportional load for each spring was set in 230 kgf or approximately 2255 N.

4.2.1.6 Discretisation and meshing

The number of elements per circle on the cross section of the wire varied depending on the geometry. The total number of elements on the spring were over 100 000 for all the models. All the elements were linear hexahedron C3D8R type. These elements are a continuum tri-dimensional eight node with reduced integration. The final meshing was suitable for this kind of analysis (Figure 4.4a). The distribution of elements on the curvature of the wire where an outer section of elements and several inner sections are set as layers, this helped to determinate the areas of bigger stress in the spring (Figure 4.4b).

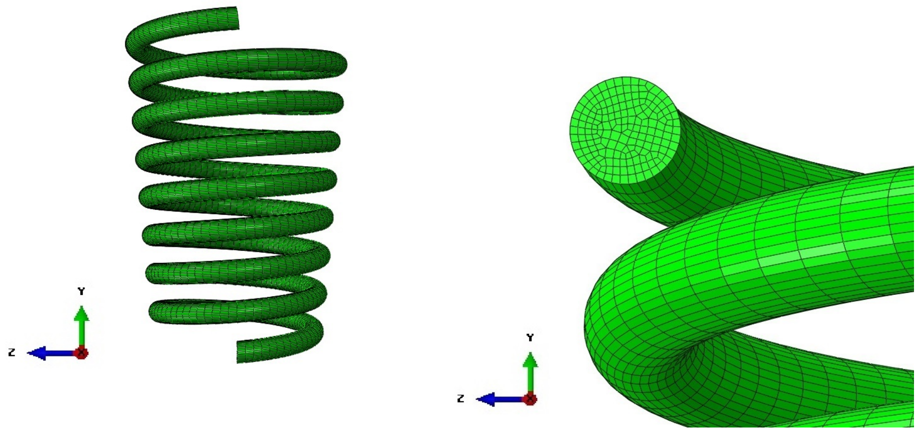

(a) Complete spring model meshed. (b) Wire mesh close-up.

Figure 4.4: Spring model S01 meshed.

The meshing of the model was made using a value of global size of seeds of 06 with a curvature control deviation value of 0.02. These values were obtained after performed simulations, with the objective to verified the results were within an acceptable range. In Figure 4.5 it is possible to observe after the increment of elements in the mesh, the results do not vary considerably.

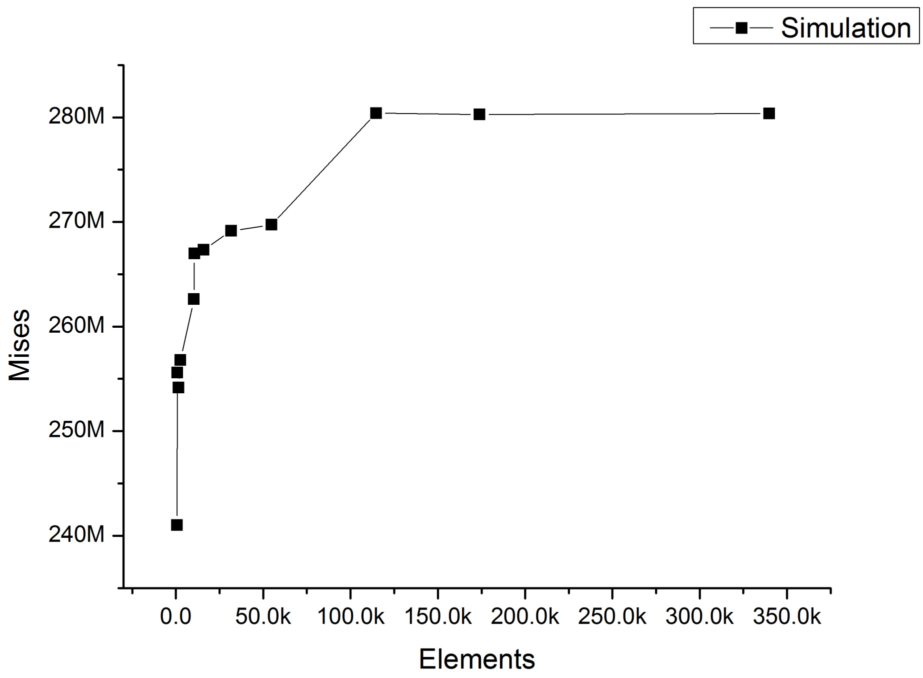

Figure 4.5: Results of simulations after increment of mesh elements

4.3 Simulations models

Three springs models were decided to be created to represent three different geometries. The simulating of the spring models had the same mesh properties, boundary conditions, magnitude and load direction, interactions and material properties. The only difference was set on the wire diameter. The diameter was defined by the material behaviour that was observed to be reduced and converted into rust in the corroded sample analysis (Section 3.3.4.3).

None of the possible pitting points or localised corrosion were included, in order to obtain a more uniform structure. Usually corrosion takes part and the inclusions or quality of the material, influence on the amount of corrosion that can appear in a specific area. The exposure time for all the spring may not be the same, and then the pitting size may vary from one to another spring. In order to maintain a simplified model, the pitting corrosion depth variables were excluded.

The spring was considered as a uniform corroded model, and the reduction was the only variation of a the wire diameter. This was chosen in order to simplify the model and to give an approach of general corrosion on the spring. Expecting a uniform corrosion in all the surface. This situation may not be the most common however it is still possible, specially if there is a problem with the protective coatings. Improvements of the model are mentioned on section 5.1.

The first spring, with a 16 mm wire diameter will be referred as S01. The second spring which has a wire diamenter of 15 mm will be referred as S02. And the last CAD model with a 14 mm wire diameter, will be referred as S03.

4.3.1 First spring simulation

The first simulation was made using spring S01 (Figure 4.6). This model had 103 999 C3D8R elements. A load of 2255 N was applied and this generated a deflection of 40.68 mm. The biggest value of stress observed, was located on the inner part of the coil (Figure 4.6c), as expected, and had a Mises stress value of 280.4 MPa (Figure 4.6a).

In some images the mesh was removed from the model for a better view as shown in Figure 4.6a. An image of the loaded spring with a cross sectional cut is presented in Figure 4.6c to improve visibility on stress distribution on the wire and coil of spring S01. In this image is possible to see how the stress is bigger on the inside of the coil and in the centre of the wire it comes to minimum values, as expected from the theory and define in Figure 2.8.

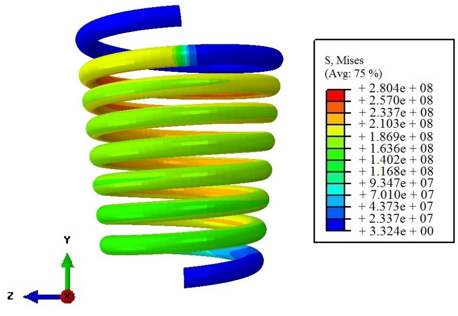

(a) Spring S01 loaded without mesh.

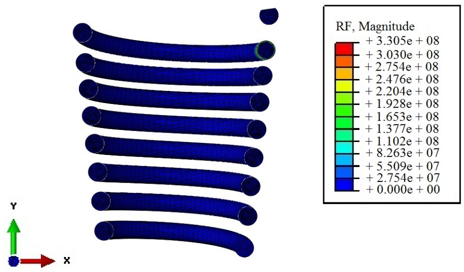

(b) Reactive force shown on a cross sectional cut of the loaded spring S01.

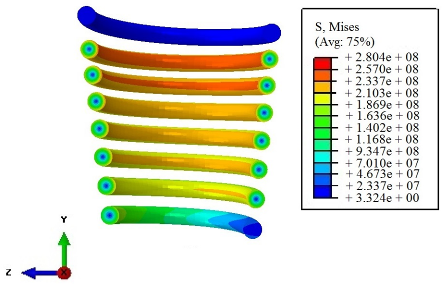

(c) Cross sectional view of the loaded spring S01 with no mesh.

Figure 4.6: Finite element model simulation for spring S01

4.3.2 Second spring simulation

On the second simulation (Figure 4.7) the boundary conditions, the load applied and the mesh configuration were kept the same. Only the reduction of 1 mm on the wire diameter was set as variable. The mesh size for this simulation was of 102 205 C3D8R elements. The total deflection of the spring was 49.27 mm and the largest Mises stress value registered on the spring was of 306.9 MPa (Figure 4.7a).

Figure 4.7c shows a cross sectional cut of the loaded spring S02. The distribution of the load tends to distribute the majority of the stress on the

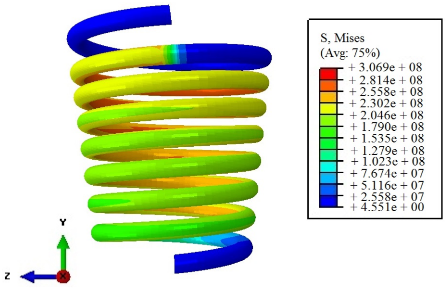

(a) Spring S02 loaded without mesh.

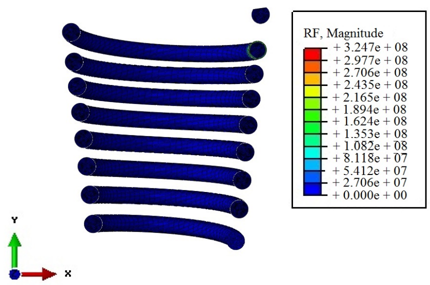

(b) Reactive force shown on a cross sectional cut of the loaded spring S02.

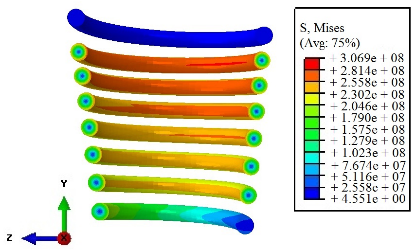

(c) Cross sectional view of the loaded spring S02 with no mesh.

Figure 4.7: Finite element model simulation for spring S02

inside of the coils.

One more time is possible to observe the critical area created on the boundary between the pinned coil and the moving coil where the reaction force (RF) create an additional stress concentration (Figure 4.7b).

4.3.3 Third spring simulation

For the third simulation spring model S03 was used (Figure 4.8), the same set up was kept, and also only the geometry from the CAD model varied in the wire diameter. In this model the geometry varied by a 2 mm reduction on the wire diameter versus the spring model S01. The same mesh set up in S03 model obtained 111 162 C3D8R elements, the largest amount of elements in all three models. The same load of 2255 N was applied. The height deflection of the spring in this case was of 60.59 mm. The calculated Mises stress value was of 351.6MPa, a higher value as the previous simulations as expected.

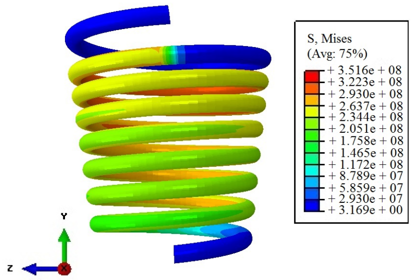

(a) Spring S03 loaded without mesh.

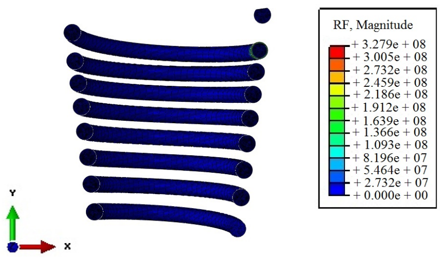

(b) Reactive force shown on a cross sectional cut of the loaded spring S03.

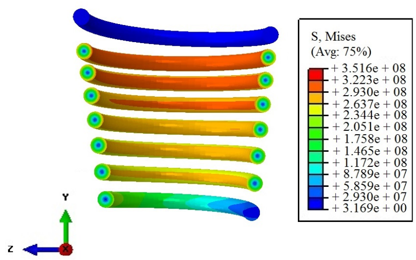

(c) Cross sectional view of the loaded spring S03 with no mesh.

Figure 4.8: Finite element model simulation for spring S03

4.3.4 Fourth spring simulation

A fourth simulation was made using spring model S03, in this simulation the load was applied from the lower coil while the top coil was pinned, as presented in Figure 4.9.

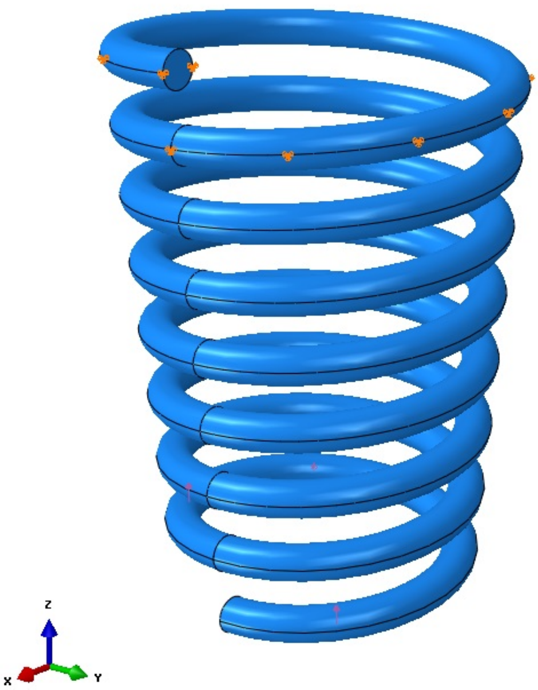

Figure 4.9: Load applied on bottom coil, top coil pinned

It was observed that in this simulation, the values were higher than those obtained on the previous simulations (Figure 4.10a). The upper coils tend to bump each other prior to reach the solid length (Figure 4.10b). It is also observable that the stress distribution on the spring is concentrated in the upper area of the spring and the value of stress are significantly higher, in this case 411.3 MPa.

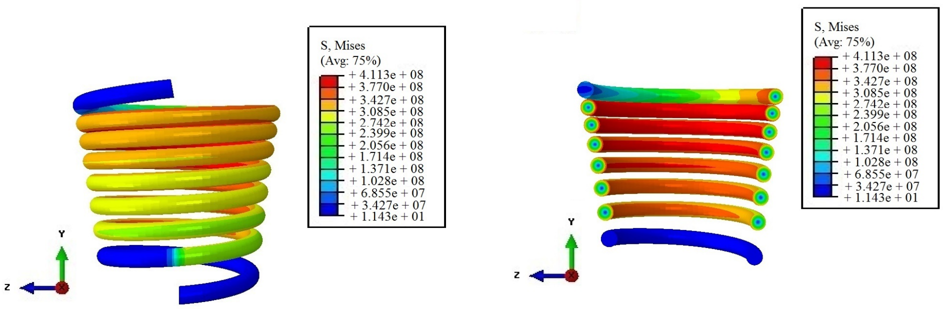

(a) Spring S03 loaded without mesh.

(b) Cross section image of spring S03.

Figure 4.10: Finite element model second simulation for spring S03.

4.3.5 Comparison of simulations

A comparison between the numerical and an analytic analysis was performed to confirm the match between the results obtained from the simulation and the theory approach. The first spring configuration was used as reference for the comparison, Table 4.3. The spring characteristics were assumed to be similar. Figure 4.11 shows the results of the loading vs. deflection on each simulation compared to the analytical results.

Table 4.3: Comparison between analytical and numerical analysis on simulation of first spring

Values obtained			
Characteristic	**Spring S01**	**Analytical**	**Difference**
Load (N)	2255	2255	0
Wire diameter (mm)	16	16	0
Total deflection (mm)	40.68	36.38	4.3
Mises value (MPa)	280.4	305.3	24.9

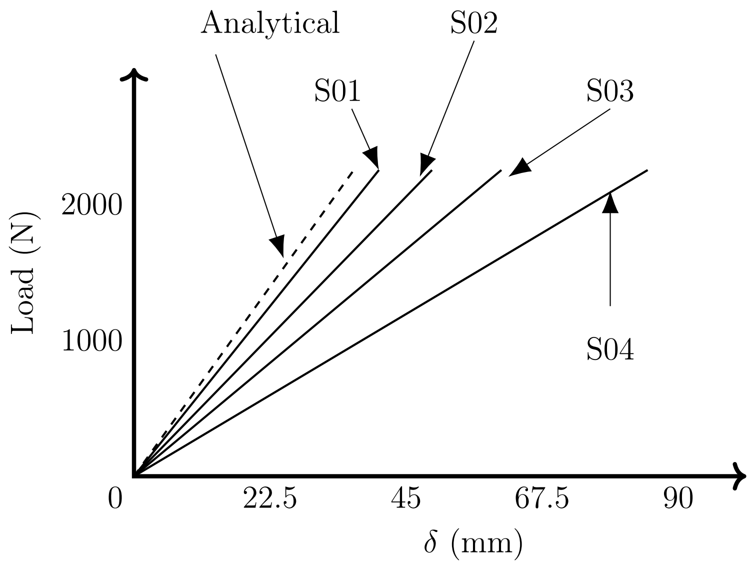

Figure 4.11: Load-deflection of spring simulation.

The parameters to compare were the total deflection and the maximum stress value. For the total deflection value the formula 2.2 was used. Using the same values for the material properties the deflection calculated was of 36.6 mm.

The maximum stress value was calculated as per formula 2.12 where the curvature factor correction factor 2.10 is included to provide the maximum value on the material for the estimated load. In this case the value obtained was 305.3 MPa.

The main difference on the analytical analysis and the numerical is the geometry can not be perfectly determined on the analytical. As mentioned the spring has a 5 degrees of aperture, meaning it is not a straight spring. However due to the simplicity of the formulas the mean diameter can not be modified for each coil which presents the differences between the results.

Table 4.4: Final simulation values for the three spring configurations

Final values of simulations				
Characteristic	**Spring S01**	**Spring S02**	**Spring S03**	**Spring S03-2**
Wire diameter (mm)	16	15	14	14
Mesh Elements	103 999	102 025	111 162	111 162
Total deflection (mm)	40.68	49.27	60.59	84.88
Mises value (MPa)	280.4	306.9	351.6	411.3

For the amount of stress generated again the lack of better representation of the geometry leads to a bad representation of the stress the material is subjected to. While the numerical analysis provide a more accurate result it is possible to redefine the design with a more precise result of the simulation.

Simulation of spring S02 presented results similar in trend of distribution of stress along the spring coils with the simulation of spring S01. Spring S02 has more area under more stress in comparison with the spring simulation of S01. The total deflection of the spring also increased by 9 mm against S01.

This trend is repeated again in simulation of the spring S03 where is possible to observe how the increase of the stress on the same areas of the upper coils are distributed. In simulation of spring S03 also the values for deflection are increased by almost 20 mm against the deflection of simulation for spring S01.

The trend of the stress behaviour on the material can be compared on the images for the cross sectional figures of the three loaded springs (Figure 4.6c 4.7c 4.8c). Table 4.4 presents the final values obtained in the simulations.

Overall is possible to recognise the trend of the spring behaviour where the upper coils are the first to sustain more stress and the deflection increases creating more stress on the material even if the load remains static. However it was found that in the second simulation of spring S03, depending on the direction of the load, this will have a different influence on the spring behaviour and therefore on the type of wear.

The second simulation of spring S03 presented higher values of Mises stress, and also bigger deflection of the spring, more than 20 mm versus the same spring model under different load condition. The upper coils tend to collide before the solid length has been reached.

This is believe to occurs based on the difference of material available to respond primarily to the load, and the change in the diameter of the pinned section. This is the perfect example of how the geometry plays an important role in spring design.

4.4 Discussion

Three CAD model springs were generated, one spring represented the optimal conditions of a homogeneous material with the properties previously mentioned and the spring was created with an ideal geometry. This model represents the spring for the suspension system as ready to take part on the assembly process of an automobile. The second spring had the same geometrical conditions, such as pitch size, mean diameter and aperture angle with the exception of the diameter reduction in the wire diameter. This spring was representing part of the material lost as being subjected to a general corrosion mechanism. The dimensions were based on the previously performed analysis on the corroded samples. This was done to verify the trend of the stress distribution and spring behaviour under loading conditions in the corroded spring. The third spring model was made with the same conditions but under an advance corroded status, the wire of the spring was considered with a more reduced diameter, to compare the results and the possible prediction of the behaviour of the spring.

The distribution of the load was simulated to have a perfect fit and the load could be represented on the coil itself. To counteract the displacement that could occur on the spring at the other end of the coil, it was assigned a pinned boundary condition. This pinned condition was chosen instead of an encastre because the later avoids the natural rotation of the material. This would only create additional shear stresses, that is not involved in a real situation.

Once the results were compared, the trend of the stress distribution was confirmed. The increase of stress in the material and the deflection of the spring increases under the same load. This was expected since the wire diameter has been reduced. This performance indicates a clear lost of the designed properties and how these values alter the expect result on the complete suspension system. If the material experiences an increase of stress on specific zones, this may generate and propagate the localized corrosion sites. These sites will create more pits and at the same time the pits will generate an additional localized stress on the material, which will lead to the material fracture.

A comparison between the third and fourth simulations was the direction of the load and the boundary conditions (the pinned coil) were inverted (Figure 4.9). It was observed that in the fourth simulation the values of stress and deflection were significantly higher (Figure 4.10a). The upper coils in the fourth simulation tended to bumped before reaching the solid length. This proved the presumption that depending on the direction of the load, it will have a different influence on the spring behaviour and wear. If coils tend to get in contact between each others it will result in a faster attrition of the protective coating and will lead to premature corrosion of the spring.

It was also noted critical area in the springs was created if the seat does not allow any movement on the spring, having a "hard seat" the reaction forces on these points would also create an additional stress concentration on the material.

4.5 Concluding remarks

The geometry of the model and the mechanical properties of the material used were significantly representative with the real component. The boundary conditions were simplified and they were expected to replicate the real life situation were possible. The discretization of the models was made under the same procedure to obtain a more related conditions between the models regardless of the amount of elements.

Simulation of the models was done with the same load of 2255 N; which is representative of the usual static load caused by the weight of a vehicle and boundary conditions. A trend of the performance was observed and this behaviour was expected; leading to believe the simulations represent correctly the material response.

A comparison between an analytic and numerical analysis was made with one of the spring configuration, finding a good correlation between these two. With only a difference of 24.9 MPa as a result of the comparison.

As seen from the images, the spring behaviour is modified even by a small reduction of the wire diameter; in these simulations the reduction was considered as 1 mm of the wire diameter. This reduction can occur if the material has been subjected to harsh environmental conditions. The comparison between the simulations presents a significantly increase of the stress that the material is exposed to. The capacity of response of the spring to avoid compression is reduced and the performance is degenerated; the deflecion increased from 40.68 mm to 60.59 mm on the most corroded model.

A final simulation was made with the exception of change between the boundary conditions and this help to prove the direction of the load also have a crucial role in the performance of the spring. This simulation obtained an additional 130.9 MPa of stress increase and 44.2 mm of added deflection.

Chapter 5

Conclusions

The mechanical principles and theorems on which the equations for calculating the dimensions of the spring were presented. It was explained what are the steps involved on the simulation of a spring, and the comparative of the simulation results against analytical stress values, displacement and spring rate presented. It is mentioned how the mechanical properties such as torsional yield strength and ultimate tensile strength are fundamental for a spring performance.

The interaction of the material with the environment in a real life application are not controllable. The imperfections, irregularities of the spring, and the impact of the environment over the springs tend to be the cause of corrosion initiation in most cases.

To avoid the corrosion in the spring analysed, an organic coating layer is used as a protection barrier; it was measured and found the thickness values range from 102-145 μm. However corrosion mechanisms; such as general corrosion, crevice corrosion and pitting corrosion, were identified in the spring. It was observed the organic coating remain intact but corrosion still appears on the spring; corrosion can propagate inside the coating layer.

Samples of the new spring were analysed, the material composition of the metallic alloy was confirmed. Samples from an aged or corroded spring were analysed as well, and it was confirmed the material composition was similar to the first spring. An example of impurity in the material that could lead to initiation of corrosion was found in one of the samples.

The spring diameter was reduced as a result of corrosion. This condition was used to generate a CAD model and later used as part of the FEM simulation. A simplified FEM simulation was made to compare the difference between the CAD models of a new spring and a corroded spring.

A simplified simulation model was made by removing the interaction between the spring and the seats and applying the load directly to the springs. The FEM simulations showed that reducing the diameter of the spring, it presents higher values of material stress. It also increase deflection to the same static load of 2255 N up to 20 mm . This stress increase can also incite more corrosion sites and eventually cause a material failure.

An analytical calculation of the spring configuration was made to compare the difference between this result and the simulation obtained from the numerical analysis. The difference was of only 24.9 MPa in stress increase for springs of the same wire diameter. The difference is presumed to be due to the difference of the geometrical shape between the numerical and analytical analysis. Finally a comparison between the simulations of different wire diameter of the spring provided evidence of a performance trend which was the expected behaviour of the spring.

Thanks to this analysis it is possible to present the deterioration of the spring performance based on the presence of corrosion on the material.

5.1 Future Work

After reviewing the process in which the spring was analysed and simulated, some changes could be made in order to improve the information used as an input of the simulation and obtain more specific results.

A modification on the geometrical model of the spring, with the target of creating a more realistic analysis of the spring behaviour. Include values of real loading in operation that will present in the life cycle of the spring.

A survey on different springs to find areas that are more prone to develop corrosion, due to wear, or damage in the life cycle. Using these results on the corrosion presence, a model could be updated to simulate these sites, giving a better representation of the mechanism of corrosion in the spring and will eventually lead to more realistic values to those presented in the spring operation.

A new simulation could be incorporated with a non-corrosive material, such a composite material and check the performance of the spring, optimizing the design based on the results obtained from these last simulations to comply with the new material mechanical properties. Using mechanical test to verify the result values of both the simulation and the analytical, and to validate the simulations of the expected performance with the new material.

Glossary

ν Poisson's ratio, is the ratio of transverse to axial strain. When a material is compressed or stretch in one direction, it usually tends to expand or contract in the other two directions perpendicular to the direction of load.. 34

E Young's modulus describes tensile elasticity, or the tendency of an object to deform along an axis when opposing forces are applied along that axis; it is defined as the ratio of tensile stress to tensile strain. It is often referred to simply as the elastic modulus.. 34

G Shear modulus or modulus of rigidity, is defined as the ratio of shear stress to the shear strain, The shear modulus is concerned with the deformation of a solid when it experiences a force parallel to one of its surfaces while its opposite face experiences an opposing force . 31, 34

S_{UT} Is the maximum stress that a material can withstand while being stretched or pulled before failing or breaking. Tensile strength is not the same as compressive strength and the values can be quite different.. 33

Acronyms

ASTM American society for testing and material. 29, 71

BS British standard. 29

CAD computer aid design. 89, 93–95, 100, 102, 108, 113

CF corrosion fatigue. 48

CFRP carbon fibre reinforced polymer. 34

DFA damage function analysis. 60

DIN Deutsches institut für normung. 29

EDX energy-dispersive x-ray spectroscopy. 64, 79, 83

EVS extreme value statistics. 60

FEA finite element analysis. 68

FEM finite element model. 57, 58, 60, 66, 68, 70, 71, 90, 91, 113

GFRP glass fibre reinforced polymer. 29

kV kilo Volts. 79

RF reaction force. 102

rpm revolutions per minute. 77

SCC stress corrosion cracking. 48, 52–54, 61, 68

SEM scanning electron microscope. 58, 64, 68, 71, 78, 84

TEM transmission electron microscope. 64

Bibliography

[1] Paz, E., Ceccarelli, M., and Otero, J. (2010) *A Brief Illustrated History of Machines and Mechanisms*.

[2] Cole, I. S., Paterson, D. A., and Ganther, W. D. (2003) Holistic model for atmospheric corrosion part 1 - theoretical framework for production, transportation and deposition of marine salts. *Corrosion Engineering, Science and Technology*, **38**, 129–134.

[3] Trenouth, W. R., Gharabaghi, B., and Perera, N. (2015) Road salt application planning tool for winter de-icing operations. *Journal of Hydrology*, **524**, 401–410.

[4] Ghassemieh, E. (2011) New trends and developments in automotive industry. pp. 366–394.

[5] (2015), The fluorinated greenhouse gases regulations 2015.

[6] (2005) The end-of-life vehicles (producer responsibility) regulations 2005.

[7] Childs, P. R. (2003) *Mechanical Design*. Elsevier.

[8] Wahl, A. M. (1944) *Mechanical springs*. Penton Publishing Company.

[9] Shigley, J. E., Budynas, R. G., and Mischke, C. R. (2004) Mechanical engineering design.

[10] Kumar, Y. N. V. S. and Teja, M. V. (2012) Design and analysis of composite leaf spring. *International Journal of Mechanical and Industrial Engineering*, **2**, 97–100.

[11] Knowles, D. (2011) *Automotive suspension steering systems*. Delmar CENGAGE.

[12] Watanabe, K., Tamura, M., Yamaya, K., and Kunoh, T. (2001) Development of a new-type suspension spring for rally cars. *Journal of Materials Processing Technology*, **111**, 132–134.

[13] Chavhan, G., Burande, S., and Dhole, L. (2014) Analysis of shock absorber using different material of spring. *International Journal of Advanced Engineering Technology*, **V**, 19–21.

[14] Ravi Kumar, B., Bhattacharya, D. K., Das, S. K., and Ghosh Chowdhury, S. (2000) Premature fatigue failure of a spring due to quench cracks. *Engineering Failure Analysis*, **7**, 377–384.

[15] (1963), Handbook of mechanical spring design.

[16] Shimoseki, M., Hamano, T., and Imaizumi, T. (eds.) (2003) *FEM for Springs*. Springer Berlin Heidelberg.

[17] Spring, A. (ed.) (1987) *Handbook, Design. Engineering Guide to Spring Design*. Barnes Group.

[18] Samónov, C. (1984), Some aspects of design of helical compression springs.

[19] Mises, R. V. (1913) Mechanics of solid bodies in the plastically-deformable state. *Math.-phys. Klasse*, **4**, 1–10.

[20] Samónov, C. (1980) Computer-aided design of helical compression springs. *ASME paper*.

[21] Heaton, H. (1896) A method of solving quadratic equations. *The American Mathematical Monthly*, **3**, 236–237.

[22] Davis, J. R. (2000) *Corrosion: Understanding the basics.*. ASM International,.

[23] Fontana, M. G. (2005) *Corrosion engineering*. Tata McGraw-Hill Education.

[24] LaQue, F. L. and Copson, H. R. (1963) *Corrosion resistance of metals and alloys*, vol. 158. Reinhold Publishing Corporation.

[25] Mac Rae, A. (1964) Adsorption of oxygen on the {111}, {100} and {110} surfaces of clean nickel. *Surface Science*, **1**, 319–348.

[26] Bernhardsson, S., Eriksson, L., Oppelstrup, J., Puigdomenech, I., and Wallin, T. (1981), 8th int. cong. on metallic corrosion.

[27] Scully, J. (1990) *The fundamentals of corrosion*. Pergamon Press, third edit edn.

[28] Betts, A. J. and Boulton, L. H. (1993) Crevice corrosion: review of mechanisms, modelling, and mitigation. *British Corrosion Journal*, **28**, 279–296.

[29] Oldfield, J. W. and Sutton, W. H. (1978) Crevice corrosion of stainless steels: I. a mathematical model. *British Corrosion Journal*, **13**, 13–22.

[30] Pickering, H. (1989) The significance of the local electrode potential within pits, crevices and cracks. *Corrosion Science*, **29**, 325–341.

[31] Karlberg, G. and Wranglen, G. (1971) On the mechanism of crevice corrosion of stainless cr steels. *Corrosion Science*, **11**, 499–510.

[32] Pourbaix, A. (1987) *Corrosion chemistry within pits, crevices and cracks*. HMSO, 1 edn.

[33] Ijsseling, F. P. (1980) Electrochemical methods in crevice corrosion testing: Report prepared for the european federation of corrosion working party 'physico-chemical testing methods of corrosion: Fundamentals and applications'. *British Corrosion Journal*, **15**, 51–69.

[34] Oldfield, J. W. (1987) Test techniques for pitting and crevice corrosion resistance of stainless steels and nickel-base alloys in chloride-containing environments. *International Materials Reviews*, **32**, 153–172.

[35] Kain, R. M., Lee, T. S., and Oldfield, J. W. (1986) *Electrochemical techniques for corrosion engineering*. NACE.

[36] Sedriks, A. J. (1979) *Corrosion of stainless steels*. Wiley.

[37] Szklarska-Smialowska, Z. (1986) *Pitting corrosion of metals*. NACE.

[38] (2011) *ASTM Standard G48, Standard Test Methods for Pitting and Crevice Corrosion Resistance of Stainless Steels and Related Alloys by Use of Ferric Chloride Solution.*. ASTM International.

[39] (2012) *ASTM G78-01, Standard Guide for Crevice Corrosion Testing of Iron-Base and Nickel-Base Stainless Alloys in Seawater and Other Chloride-Containing Aqueous Environments*. ASTM International.

[40] Kain, R. M. (1984) Mater. perform. **23**, 24.

[41] Wang, H. and Han, E.-H. (2013) Simulation of metastable corrosion pit development under mechanical stress. *Electrochimica Acta*, **90**, 128–134.

[42] Isaacs, H. S. (1988), Initiation of stress corrosion cracking of sensitized type 304 stainless steel in dilute thiosulfate solution.

[43] Kondo, Y. (1989) Prediction of fatigue crack initiation life based on pit growth. *Corrosion*, **45**, 7–11.

[44] Weibull, W. (1961) *Fatigue Testing and Analysis of Results*. Elsevier.

[45] Turnbull, A. and Zhou, S. (2004) Pit to crack transition in stress corrosion cracking of a steam turbine disc steel. *Corrosion Science*, **46**, 1239–1264.

[46] (1988) *ASTM A294, Specification for Alloy Steel Forgings for Turbine Wheels and Disks*. ASTM International.

[47] Turnbull, A., McCartney, L., and Zhou, S. (2006) Modelling of the evolution of stress corrosion cracks from corrosion pits. *Scripta Materialia*, **54**, 575–578.

[48] Turnbull, A., Horner, D., and Connolly, B. (2009) Challenges in modelling the evolution of stress corrosion cracks from pits. *Engineering Fracture Mechanics*, **76**, 633–640.

[49] Horner, D. A., Connolly, B. J., Zhou, S., Crocker, L., and Turnbull, A. (2011) Novel images of the evolution of stress corrosion cracks from corrosion pits. *Corrosion Science*, **53**, 3466–3485.

[50] Salvo, L., Cloetens, P., Maire, E., Zabler, S., Blandin, J., Buffière, J., Ludwig, W., Boller, E., Bellet, D., and Josserond, C. (2003) X-ray micro-tomography an attractive characterisation technique in materials science. *Nuclear Instruments and Methods in Physics Research Section B: Beam Interactions with Materials and Atoms*, **200**, 273–286.

[51] Chastell, D., Doig, P., Flewitt, P., and Ryan, K. (1979) The influence of stress on the pitting susceptibility of a 12%crmov martensitic stainless steel. *Corrosion Science*, **19**, 335–341.

[52] Suter, T., Webb, E. G., Bohni, H., and Alkire, R. C. (2001), Pit initiation on stainless steels in 1 m nacl with and without mechanical stress.

[53] De Cogan, D. (2000) Cellular automata modelling of physical systems, by bastien chopard & michel droz, cambridge university press (aléa saclay collection), 336 pp., isbn 0-521-46168-5, hardback, £55. *International Journal of Numerical Modelling: Electronic Networks, Devices and Fields*, **13**, 75.

[54] von Neumann, J. (1966) *Theory of Self-Reproducing Automata*.

[55] Chopard, B., Frachebourg, L., and Droz, M. (1994) Multiparticle lattice gas automata for reaction diffusion systems. *International Journal of Modern Physics C*, **05**, 47–63.

[56] Gutman, E. M. (1998) *Mechanochemistry of materials*. Cambridge Int Science Publishing.

[57] Engelhardt, G. and Macdonald, D. D. (2004) Unification of the deterministic and statistical approaches for predicting localized corrosion damage. i. theoretical foundation. *Corrosion Science*, **46**, 2755–2780.

[58] Luther, T. and Könke, C. (2009) Polycrystal models for the analysis of intergranular crack growth in metallic materials. *Engineering Fracture Mechanics*, **76**, 2332–2343.

[59] Aurenhammer, F. (1991) Voronoi diagrams—a survey of a fundamental geometric data structure. *ACM Comput. Surv*, **23**, 345–405.

[60] Jivkov, A., Stevens, N., and Marrow, T. (2006) A three-dimensional computational model for intergranular cracking. *Computational Materials Science*, **38**, 442–453.

[61] Gertsman, V. and Bruemmer, S. (2001) Study of grain boundary character along intergranular stress corrosion crack paths in austenitic alloys. *Acta Materialia*, **49**, 1589–1598.

[62] Luo, C., Zhou, X., Thompson, G., and Hughes, A. (2012) Observations of intergranular corrosion in aa2024-t351: The influence of grain stored energy. *Corrosion Science*, **61**, 35–44.

[63] Wenman, M., Trethewey, K., Jarman, S., and Chard-Tuckey, P. (2008) A finite-element computational model of chloride-induced transgranular stress-corrosion cracking of austenitic stainless steel. *Acta Materialia*, **56**, 4125–4136.

[64] Berger, C. and Kaiser, B. (2006) Results of very high cycle fatigue tests on helical compression springs. *International Journal of Fatigue*, **28**, 1658–1663.

[65] Rokhlin, S., Kim, J., Nagy, H., and Zoofan, B. (1999) Effect of pitting corrosion on fatigue crack initiation and fatigue life. *Engineering Fracture Mechanics*, **62**, 425–444.

[66] Paris, P., Gomez, M., and Anderson, W. (1961) A rational analytic theory of fatigue. *Trend Engineering*, **13**, 9–14.

[67] Aggarwal, M. L., Agrawal, V. P., and Khan, R. A. (2006) A stress approach model for predictions of fatigue life by shot peening of en45a spring steel. *International Journal of Fatigue*, **28**, 1845–1853.

[68] Zhou, X., Thompson, G., and Scamans, G. (2003) The influence of surface treatment on filiform corrosion resistance of painted aluminium alloy sheet. *Corrosion Science*, **45**, 1767–1777.

[69] Pyttel, B., Brunner, I., Kaiser, B., Berger, C., and Mahendran, M. (2014) Fatigue behaviour of helical compression springs at a very high number of cycles – investigation of various influences. *International Journal of Fatigue*, **60**, 101–109.

[70] Turnbull, A., Wright, L., and Crocker, L. (2010) New insight into the pit-to-crack transition from finite element analysis of the stress and strain distribution around a corrosion pit. *Corrosion Science*, **52**, 1492–1498.

[71] Pidaparti, R. M. and Rao, A. S. (2008) Analysis of pits induced stresses due to metal corrosion. *Corrosion Science*, **50**, 1932–1938.

[72] Zhao, L., Odowd, N., and Busso, E. (2006) A coupled kinetic-constitutive approach to the study of high temperature crack initiation in single crystal nickel-base superalloys. *Journal of the Mechanics and Physics of Solids*, **54**, 288–309.

[73] Zhu, Y., Wang, Y., and Huang, Y. (2014) Failure analysis of a helical compression spring for a heavy vehicle's suspension system. *Case Studies in Engineering Failure Analysis*, **2**, 169–173.

[74] (2007) *GB/T1222-2007, Spring steels*. China Standard Express.

[75] Jivkov, A., Stevens, N., and Marrow, T. (2006) A two-dimensional mesoscale model for intergranular stress corrosion crack propagation. *Acta Materialia*, **54**, 3493–3501.

[76] Palumbo, G., King, P., Aust, K., Erb, U., and Lichtenberger, P. (1991) Grain boundary design and control for intergranular stress-corrosion resistance. *Scripta Metallurgica et Materialia*, **25**, 1775–1780.

[77] Gertsman, V., Janecek, M., and Tangri, K. (1996) Grain boundary ensembles in polycrystals. *Acta Materialia*, **44**, 2869–2882.

[78] Lehockey, E., Brennenstuhl, A., and Thompson, I. (2004) On the relationship between grain boundary connectivity, coincident site lattice boundaries, and intergranular stress corrosion cracking. *Corrosion Science*, **46**, 2383–2404.

[79] Jivkov, A., Stevens, N., and Marrow, T. (2005) *Simulation of electrochemical processes*. WIT Press.

[80] Kumar, B. R., Das, S. K., and Bhattacharya, D. K. (2003) Fatigue failure of helical compression spring in coke oven batteries. *Engineering Failure Analysis*, **10**, 291–296.

[81] Prawoto, Y., Ikeda, M., Manville, S. K., and Nishikawa, A. (2008) Design and failure modes of automotive suspension springs. *Engineering Failure Analysis*, **15**, 1155–1174.

[82] (1999) *ASTM G66-99, Standard Test Method for Visual Assessment of Exfoliation Corrosion Susceptibility of 5XXX Series Aluminum Alloys (ASSET Test)*. ASM International,.

[83] Rao, A., Whitton, J., and Kaminsky, M. (1981) Suppression of repetitive surface exfoliation of inconel 625 implanted sequentially with helium ions of different energies (20–100 kev). *Journal of Nuclear Materials*, **103**, 397–401.

[84] Del Llano-Vizcaya, L., Rubio-González, C., Mesmacque, G., and Cervantes-Hernández, T. (2006) Multiaxial fatigue and failure analysis of helical compression springs. *Engineering Failure Analysis*, **13**, 1303–1313.

[85] Fatemi, A. and Socie, D. F. (1988) A critical plane approach to multiaxial fatigue damage including out-of-phase loading. *Fatigue & Fracture of Engineering Materials & Structures*, **11**, 149–165.

[86] Wang, C. and Brown, M. (1993) A path-independent parameter for fatigue under proportional and non-proportional loading. *Fatigue & Fracture of Engineering Materials & Structures*, **16**, 1285–1297.

[87] Socie, D. and Marquis, G. (2000) *Multiaxial fatigue*. SAE International.

[88] (2010) *ASTM A401 / A401M - 10, Specification for Steel Wire, Chromium-Silicon Alloy*. ASTM International.

[89] Zipperian, D. C. (2006), Metallographic specimen preparation basics.

[90] (2002), Bs en 10089:2002, hot rolled steels for quenched and tempered springs. technical delivery conditions.

[91] Leng, Y. (2008) Scanning electron microscopy. *Materials Characterization*, pp. 121–144, John Wiley & Sons (Asia) Pte Ltd.

[92] Clough, R. (1960) The finite element method in plane stress analysis. *Proceedings of the Second ASCE Conference on Electronic Computation*.

[93] Zienkiewicz, O. and Taylor, R. (2000) *The Finite Element Method*. Butterworth Heinemann, fifth edn.

[94] Allen, D. N. d. G. (1954) *Relaxation Methods*. McGraw-Hill.

[95] Crandall, S. H. (1956) *Engineering analysis: a survey of numerical procedures*. Engineering societies monographs, McGraw-Hill.

[96] Finlayson, B. (1972) *The method of weighted residuals and variational principles, with application in fluid mechanics, heat and mass transfer*. Mathematics in Science and Engineering, Elsevier Science.

[97] McHenry, D. (1943) A lattice analogy for the solution of plane stress problems. *J. Inst. Civ. Eng.*, **21**, 59–82.

[98] Hrenikoff, A. (1941) Solutions of problems in elasticity by the framwork method. *J. Appl. Mech*, **A8**, 169–175.

[99] Newmark, N. (1949) Numerical methods of analysis in bars, plates and elastic bodies. Grinter, L. (ed.), *Numerical Methos in analysis in engineering*, Macmillan.

[100] Southwell, R. (1946) *Relaxation Methods in Theoretical Physics*. No. v. 1 in The Oxford engineering science series, The Clarendon Press.

[101] Lindeburg, M. R. (2013) *Mechanical engineering reference manual for the PE exam*. www. ppi2pass. com.